LLM Probability Concentration: How Alignment Shrinks the Generative Horizon

Anonymous authors
Paper under double-blind review

Abstract

Despite their impressive capabilities, aligned large language models (LLMs) often generate outputs that lack diversity. What drives this consistency in the generation? We investigate this phenomenon through the lens of probability concentration in the model's output distribution. To quantify this concentration, we introduce the *Branching Factor* (BF)–a token-invariant measure of the effective number of plausible next steps during generation. Our empirical analysis reveals two key findings: (1) BF often decreases as generation progresses, suggesting that LLMs become more predictable as they generate. (2) alignment tuning substantially sharpens the model's output distribution from the outset, reducing BF by a factor of 2–5 overall, and up to an order of magnitude (e.g., from 12 to 1.2) at the beginning positions. This stark reduction helps explain why aligned models often appear less sensitive to decoding strategies. Building on this insight, we find this consistency has surprising implications for complex reasoning. Aligned Chain-of-Thought (CoT) models (e.g., DeepSeek-distilled models), for instance, leverage this effect; by generating longer reasoning chains, they push generation into later, more deterministic (lower BF) stages, resulting in more stable outputs. We hypothesize that alignment tuning does not fundamentally change a model's behavior, but instead steers it toward stylistic tokens (e.g., "Sure") that unlock low-entropy trajectories already present in the base model. This view is supported by nudging experiments, which show prompting base models with such tokens can similarly reduce BF. Together, our findings establish BF as a powerful diagnostic for understanding and controlling LLM outputs - clarifying how alignment reduces variability, how CoT promotes stable generations, and how base models can be steered away from diversity.

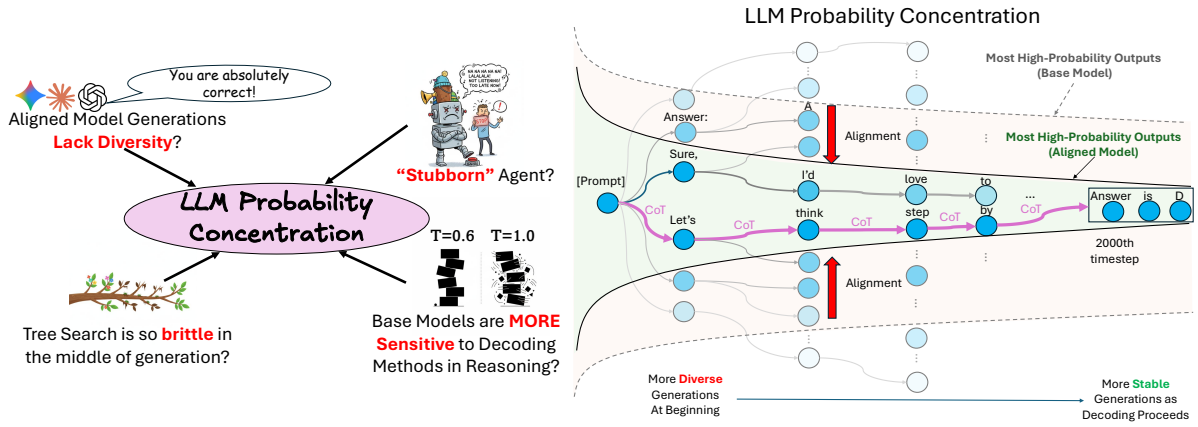

(a) (b)

Figure 1: (a): LLM probability concentration connects and explains several disparate yet critical phenomena in aligned LLMs. (b): A conceptual illustration of how alignment and CoT influence the generation space of LLMs. While base models begin with high output diversity, alignment tuning sharply concentrates early probability mass, leading to more stable outputs. CoT extends this effect into later positions, flattening output sample variation and reducing sensitivity to decoding.

1 Introduction

While alignment tuning improves helpfulness and safety in large language models (LLMs), it often introduces a trade-off: reduced output diversity (Padmakumar & He, 2024; Chakrabarty et al., 2024; Tian et al., 2024; Kirk et al., 2024; Lu et al., 2025) and increased determinism (Saparov & He, 2023; Song et al., 2024; Renze & Guven, 2024; Bigelow et al., 2024; West & Potts, 2025). As a result, aligned models are frequently observed to be less sensitive to different decoding strategies—a phenomenon we confirm in our own case study (§ 5.1). Similarly, Chain-of-Thought (CoT) prompting (Wei et al., 2022), while enhancing reasoning, often reduces the variance of answers. These observations point toward a common underlying phenomenon: *LLM Probability Concentration* (Figure 1a), where the model's vast potential output space collapses into a narrow set of likely trajectories.

But how should we rigorously conceptualize and measure this concentration? Autoregressive generation is inherently a traversal through a *branching tree* (Figure 1b). Standard metrics often fail to capture the global structure of this tree. Token-level entropy is too local; "model perplexity" (Jurafsky & Martin, 2025) measures fit to a reference dataset rather than the model's own generative breadth; and surface-level diversity metrics (e.g., n-gram diversity) are often confounded by vocabulary size and output length.

To address this, we operationalize a principled concept from information theory: *distribution perplexity* (or exponentiated entropy). Specifically, we define the **Branching Factor (BF)** as the *length-normalized* distribution perplexity (i.e., exponentiated entropy rate). This metric quantifies the effective number of viable next-token choices available to the model on average, providing a "microscopic" lens on the tree's expansion rate. Crucially, we do not propose BF as a novel mathematical metric; rather, we introduce it as a unifying framework to quantify LLM probability concentration. By leveraging the asymptotic closeness between length-averaged log-probability and entropy (Mudireddy et al., 2024), we can estimate BF efficiently from the model's own naturally sampled sequences, avoiding the need for teacher forcing or exhaustive enumeration.

The core contribution of this work is using the BF framework to provide a *unified explanation* for disparate LLM behaviors. We show that seemingly unconnected phenomena, reduced diversity in alignment, decoding insensitivity, and CoT stability, are all manifestations of probability concentration dynamics. Specifically:

① **Alignment Constrains the Branching Space:** We find that alignment tuning (e.g., RLHF) significantly reduces BF, typically by a factor of 2–5 overall, and up to an order of magnitude (e.g., $12 \rightarrow 1.2$) at the beginning positions, depending on alignment intensity. This reduction provides a quantitative mechanism for why aligned models are so insensitive to decoding parameters: there are simply fewer viable branches to prune.

② **Dynamic Concentration and CoT Stability:** We observe that BF typically declines over the course of generation, indicating that models "commit" to narrower trajectories as they generate. This explains the stabilizing effect of Chain-of-Thought: by encouraging long reasoning chains, CoT pushes the critical answer generation into later, lower-BF regions of the tree, resulting in more deterministic outcomes.

③ **Alignment Surfaces Latent Low-Entropy Paths:** Finally, we investigate *how* alignment achieves this concentration. Through "nudging" experiments, we show that conditioning a base model on a short, aligned-style prefix is sufficient to trigger a rapid drop in BF. This suggests that alignment does not fundamentally reshape the model's manifold but rather steers generation toward low-entropy subspaces that are already latent in the pre-trained model.

In summary, by viewing generation through the lens of BF, we move beyond reporting *that* aligned models are less diverse, to explaining *how* this concentration emerges from the underlying probabilistic structure.

2 Background

Autoregressive Language Models. LLMs are typically trained to predict the next token and the probability of output $P(y_{1:N}|x;\theta)$ can be decomposed as: $P(y_{1:N}|x;\theta) = \Pi_{t=1}^{N} P(y_t|[x, y_{1:t-1}];\theta)$, where $y_{1:t-1}$ is the output up to position $t-1$, θ is the model parameter, and x is the prompt (treated as fixed). Each output

sample is generated via token-by-token sampling, and the generation of multiple samples naturally forms a search tree (Yao et al., 2023; Hao et al., 2023; Wan et al., 2024). Modern LLMs go through multiple training stages. In this paper, we would use *base models* to refer to the models trained without *alignment tuning* techniques (Touvron et al., 2023), including instruction tuning and Reinforcement Learning from Human Feedback (RLHF) (Ouyang et al., 2022; Bai et al., 2022) (e.g., "Llama-2-13B" (Touvron et al., 2023)) and *aligned models* to refer to models undergoing these additional fine-tuning stages (e.g., "Llama-2-13B-Chat").

LLM Decoding and Entropy. Though LLMs are trained with a large vocabulary size $|V|$, the desired tokens often concentrate on a much smaller set of tokens under distribution $P(y_t|x, y_{1:t-1}; \theta)$. Common decoding methods (Holtzman et al., 2020; Hewitt et al., 2022) utilize this observation and propose various heuristics to truncate vocabulary V as V_t at each step t. The next token is then sampled from the renormalized distribution $\tilde{P}\left(y_t|[x, y_{1:t-1}]; \theta\right) = \mathbb{1}(y_t \in V_t)\frac{P(y_t|x,y_{1:t-1};\theta)}{\sum_{y_t \in V_t} P(y_t|x,y_{1:t-1};\theta)}$. Since tokens are sampled from the truncated distribution $\tilde{P}$,[1] we use $\tilde{P}$ to compute the empirical (token-level) entropy $\tilde{H}$ for a given prefix instance $y_{1:t-1}$:[2]

$$\tilde{H}\left(\mathrm{Y}_t|[x, y_{1:t-1}]; \theta\right) = -\sum_{y_t} \tilde{P}\left(y_t|[x, y_{1:t-1}]; \theta\right) \log \tilde{P}\left(y_t|[x, y_{1:t-1}]; \theta\right) \tag{1}$$

Note that $\tilde{H}$ is a *random variable* that depends on the specific realization of the prefix sequence $Y_{1:t-1} = y_{1:t-1}$. The more common notion of *conditional entropy* is thus the expectation of $\tilde{H}$ over all possible $y_{1:t-1}$:

$$\tilde{H}\left(\mathrm{Y}_t|[x, \mathrm{Y}_{1:t-1}]; \theta\right) = \mathbb{E}_{y_{1:t-1}} \tilde{H}\left(\mathrm{Y}_t|[x, y_{1:t-1}]; \theta\right) \tag{2}$$

Conventionally, we use uppercase Y to denote the *random variable* for an output and lowercase y for its specific realization. Finally, along a realized sequence $y_{1:t-1}$, we define the *realized entropy* as[3]

$$h_{\text{realized}}(y_{1:N}) \stackrel{\text{def}}{=} \sum_{t=1}^{N} \tilde{H}(\mathrm{Y}_t|y_{1:t-1}; \theta). \tag{3}$$

This metric and its sequence-level reductions (e.g., mean pooling) are of profound practical importance: while estimating the full conditional entropy $\tilde{H}(\mathrm{Y}_t|x; \mathrm{Y}_{<t})$ requires marginalizing over an exponential space of prefix trajectories, h_{realized} serves as the widely-adopted tractable proxy for quantifying generation uncertainty (Kuhn et al., 2023; Farquhar et al., 2024), generation diversity and creativity (Dušek et al., 2020; West & Potts, 2025) and controlling exploration in RLVR (Cheng et al., 2025; Cui et al., 2025; Wang et al., 2025).[4] Linearity of expectation and the chain rule for entropy then gives us

$$\mathbb{E}_{y_{1:N}}\left[h_{\text{realized}}(y_{1:N})\right] = \sum_{t=1}^{N} \tilde{H}\left(\mathrm{Y}_t|[x, \mathrm{Y}_{1:t-1}]; \theta\right) = \tilde{H}(Y_{1:N}|x; \theta), \tag{4}$$

i.e. h_{realized} is an unbiased estimator of the marginal entropy of the whole generative process.

A Note on Practical Text Generation. Throughout this paper, we model an LLM as generating sequences of a fixed maximum length N, with realizations denoted by $y_{1:N}$, and some theoretical results consider the asymptotic regime $N \to \infty$. In practice, however, generation often terminates early, producing a shorter sequence $y_{1:n}$ with $n < N$. Our framework accommodates this by defining an *equivalent sequence* $\hat{y}_{1:N}$ such that $\hat{y}_t = y_t$ for $t \leq n$, and $\hat{y}_{n+1:N}$ consists of repeated special tokens (e.g., EOS) indicating termination. We further assume $\tilde{P}\big(Y_{n+1:N} = \hat{y}_{n+1:N} \mid [x, y_{1:n}]; \theta\big) = 1$, which can be viewed as a property of pretrained LLMs. Under this convention, the probability of the equivalent sequence satisfies $\tilde{P}(\hat{y}_{1:N} \mid x; \theta) = \tilde{P}(y_{1:n} \mid x; \theta)$. Consequently, without loss of generality, we may treat all generations as having length N.

[1] Our main experiments employ mild decoding settings (T=1.0, p=0.9). These settings approximate the full distribution, align with standard evaluation practices, and ensure coherent generation from base models. Stronger truncation settings are explicitly noted where applied.

[2] The common convention setting $0 \log 0 = 0$ for entropy computation is followed.

[3] For notational brevity, we hereafter omit explicit conditioning on the input x when the context is clear.

[4] See more related work discussions in § 7

3 Measuring LLM Branching Factor

Probability Concentration and the Branching Factor. The generative process of language models can be viewed as moving down a branching tree, with each token choice selecting a path forward. While the theoretical search space spans $O(|V|^N)$ sequences for vocabulary size $|V|$ and fixed sequence length N, LLMs concentrate the vast majority of probability mass on a much smaller subset of trajectories (Holtzman et al., 2020; Hewitt et al., 2022). This high-probability subset forms a complex, sparse "effective tree" $\mathcal{T}$.

To quantify the size of this effective tree, we utilize the concept of exponentiated entropy (perplexity). We define the effective set size $|\mathcal{T}|$ as:

$$|\mathcal{T}| \stackrel{\text{def}}{=} \exp\left(\tilde{H}(Y_{1:N}|x;\theta)\right). \tag{5}$$

Information-theoretically, $|\mathcal{T}|$ reflects the size of a uniform distribution (a "fair die") that would possess the same total uncertainty (entropy) as the model's actual complex distribution over sequences of length N (O'Connor, 2013).

Defining Branching Factor via Balanced Tree Model. Because the exact topology of the effective tree $\mathcal{T}$ is irregular and intractable, we map it to an *equivalent balanced B-ary tree* of the same depth N. A perfectly balanced tree with constant branching factor B and depth N contains B^N leaf nodes. By equating this theoretical leaf count to the effective set size ($B^N = |\mathcal{T}|$), we derive the **Branching Factor (BF)** as the geometric mean of the branching width:

$$B \equiv B(x;\theta) \stackrel{\text{def}}{=} |\mathcal{T}|^{1/N} = \exp\left(\frac{1}{N}\tilde{H}(Y_{1:N}|x;\theta)\right) = \exp\left(\bar{H}(Y_{1:N}|x;\theta)\right) \tag{6}$$

where $\bar{H}(Y_{1:N}|x;\theta)$ denotes the length-averaged marginal entropy of the sequence. $B(x;\theta)$ thus provides a normalized, token-invariant metric: it quantifies the effective number of plausible next-token choices available to the model on average at any given step.

Linking Entropy and Log-Likelihood in Long Sequences. Calculating the exact Branching Factor requires the total entropy $\tilde{H}(Y_{1:N}|x;\theta)$. As discussed in § 2, computing this quantity directly is intractable due to the exponential number of possible trajectories. A standard Monte Carlo approach uses the *realized entropy* $h_{\text{realized}}(y_{1:N})$ of sampled sequences as a proxy. Since h_{realized} is an unbiased estimator (Eq. 4), averaging it over sufficient samples converges to the true total entropy.

However, for long sequences, even calculating h_{realized} becomes computationally prohibitive. It requires a full summation over the vocabulary V at every generation step to compute the local entropy, incurring a total cost of $O(N \cdot |V|)$. In contrast, computing the sequence's negative log-likelihood (NLL) involves only the probabilities of the selected tokens, scaling linearly as $O(N)$. To enable efficient estimation for long horizons, we effectively need a second level of approximation: using the computationally cheap NLL as a proxy for the realized entropy.

Standard Asymptotic Equipartition Property (AEP) theory (Shannon, 1948) suggests that for stationary processes, the length-averaged NLL of a typical sequence will converge to the (length-averaged) total entropy. However, LLM generation is neither stationary nor ergodic. Fortunately, Mudireddy et al. (2024) demonstrate that a robust connection persists without these strict assumptions: the NLL converges to the *realized entropy* h_{realized} instead. We characterize this relationship as follows:[5]

Theorem 3.1 (Log-Likelihood Convergence for LLMs) *Given $0 < \epsilon < 1$, as $N \to \infty$:*

$$P\left(\left|-\frac{1}{N}\log \tilde{P}\left(y_{1:N}|x;\theta\right) - \frac{1}{N}h_{realized}(y_{1:N})\right| < \epsilon\right) \to 1 \tag{7}$$

Since $\mathbb{E}[h_{\text{realized}}] = \tilde{H}(Y_{1:N}|x;\theta)$, this theorem justifies using the NLL of sampled sequences as a *proxy* for realized entropy in long horizons, provided the variance is low. As an empirical verification for Theorem 3.1, we plot NLL and realized entropy for sampled outputs of Llama-3-8B-Instruct over multiple datasets[6] in

[5] We provide a simplified proof in § H with minor changes to the original proof of Mudireddy et al. (2024). Notably, our goal is only to show the approximation between length-averaged log-likelihood and entropy for a typical sequence, so we do not require stricter assumptions like ergodicity or stationarity.

[6] For dataset-specific details, we refer readers to § B.

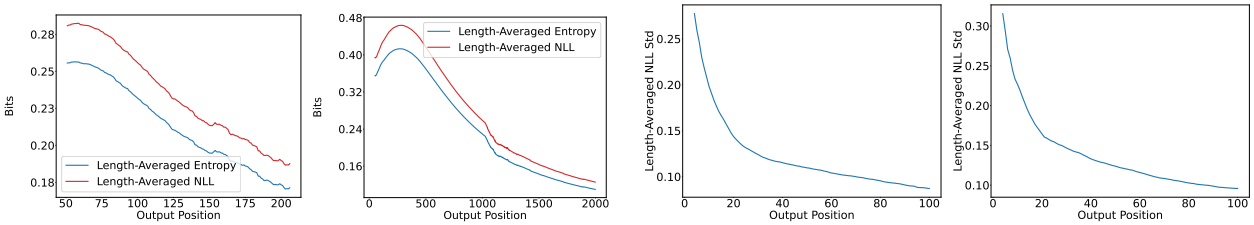

(a) MMLU (b) BBCNewsLatest (c) MMLU (Std) (d) BBCNewsLatest (Std)

Figure 2: **Convergence of NLL and Entropy.** (**a, b**): The length-averaged NLL closely tracks the length-averaged Entropy. (**c, d**): The standard deviation of the length-averaged NLL diminishes rapidly with output length.

Figure 2. We observe that: as output length increases, the deviation between NLL and realized entropy vanishes, and the standard deviation of the estimator diminishes rapidly (within the first 10 tokens).

Empirical Estimator for Branching Factor. We now translate the theoretical definition of $B(x;\theta)$ into a practical estimator $\tilde{B}(x;\theta)$. This requires addressing two practical realities: (1) we rely on finite Monte-Carlo samples rather than full distribution access, and (2) while our theory assumes a fixed N, generation in practice terminates dynamically upon emitting an EOS token.

We estimate BF using M independent sampled sequences $y^{(1)}, \ldots, y^{(M)}$. To handle the computational constraints described above, we adopt a *hybrid estimator*. For short sequences, we compute the exact realized entropy $\tilde{H}(Y_{1:|y|}|x;\theta)$ at every step (since the vocabulary is truncated to V_t, this is tractable). To avoid the GPU memory bottleneck of computing the full distribution for long sequences, we approximate entropy using NLL, a substitution justified by Theorem 3.1.

We define the estimator $\tilde{B}(x;\theta)$ by averaging over the sampled trajectories:

$$\tilde{B}(x;\theta) \approx \exp\left(\frac{1}{M}\sum_{i=1}^{M}\mathcal{E}(y^{(i)})\right), \quad \mathcal{E}(y) = \begin{cases} \frac{1}{|y|}h_{\text{realized}}(Y_{1:|y|}|x;\theta) & \text{if } |y| < L_\tau \\ -\frac{1}{|y|}\log \tilde{P}(y|x;\theta) & \text{otherwise} \end{cases} \tag{8}$$

where $|y|$ is the realized length of the sample (up to EOS) and L_τ is a threshold length. Note that explicitly normalizing by the realized length $|y|$ adapts our fixed-N theory to variable-length practice, effectively measuring the branching rate per *active* generation step.

Finally, to obtain the task-level Branching Factor, we average over the dataset X: $\tilde{B}(X;\theta) = \sum_x p(x)\tilde{B}(x;\theta)$. Unless otherwise specified, BF refers to this dataset-level branching factor in the following sections.

4 Benchmarking and Attributing Branch Factors

Models and Sampling. We run experiments on models from Llama-2 (Touvron et al., 2023) and Llama-3 (Dubey et al., 2024) families as they are widely-used open-weight model families. For each model family, we include both base and aligned models to investigate how alignment tuning affects BF. We set p=0.9 and T=1.0 to sample outputs to conform with the setting for most datasets.

We set M=50 sequences to estimate BF, which yields a reliable estimation across datasets in prior studies. For aligned models, we apply the official chat templates to prompts. In addition, we carefully control the lengths of all inputs plus outputs to be within the context window of the models.

Tasks. We consider a variety of tasks covering common application scenarios of LLM generation, including reasoning and open-ended generation: MMLU (Hendrycks et al., 2021) (Reasoning), Cognac (Chen et al., 2022) (Controlled Generation), BBCLatestNews (Li et al., 2024b) (News Generation), and Creative StoryGen (Chakrabarty et al., 2024) (Creative Generation). To test subjective randomness bias (Bigelow et al., 2024), we also prepare a synthetic task Random Strings where the prompt is generated via random characters. See § B for dataset details.

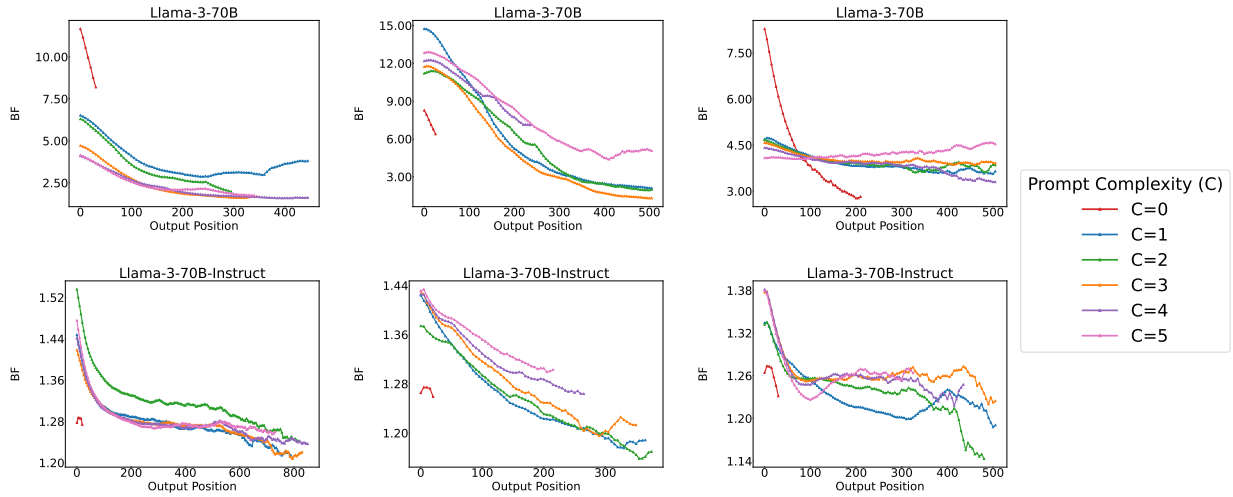

(a) Creative StoryGen (b) Random Strings (c) BBCNewsLatest

Figure 3: **Shrinking BF with output length over various tasks for Llama-3-70B and Llama-3-70B-Instruct.** For better visualization, we compute the exponential moving averaged values of BF with the smoothing factor set as 0.1.

Impact Factors (IFs). We consider modulating these factors that may impact BF computations: Prompt Complexity (C), Alignment Tuning ($AT \in \{\text{Instruct}, \text{Base}\}$), Model Size ($S \in \{8\text{B}/13\text{B}, 70\text{B}\}$), and Model Generation ($G \in \{\text{Llama-2, Llama-3}\}$). C controls the informativeness of the input prompt x (e.g., the number of banned words in Cognac, the number of in-context samples in MMLU). Intuitively, providing more information in x should make the model more confident in its outputs, resulting in a lower BF. Dataset-specific setups for C are detailed in § B. AT, S, G represent model-wise variations to explore how different configurations of θ affect $B(\text{X}; \theta)$.

4.1 BF Dynamic in Generation Process

Both BF and the output length N are functions of the output Y, and BF computation relies on N. To avoid confounding effects, we first analyze how BF varies with N before intervening IFs. In Figure 3, we demonstrate BF trajectories over different output positions by running Llama-3-70B and Llama-3-70B-Instruct on three representative tasks. Specifically, we compute BF over every five output tokens, conditioning on the prompt and all previously generated output tokens.[7] Our findings also generalize to summarization, multilingual tasks, OLMo-2 (OLMo et al., 2024) /Qwen family (Qwen, 2025) (§ G).

As we can see, first, **the base model's BF is often significantly higher than the aligned models, roughly 2–5 times**. The nearly order-of-magnitude difference is also a frequent pattern in strongly aligned models when we compare base and aligned models at the beginning of outputs. Therefore, there are actually very few candidate next-token to be truncated in decoding for the aligned models. This explains why the decoding methods exert weaker effects for aligned models (Song et al., 2024; Renze & Guven, 2024; Shi et al., 2024a), as we will see in § 5.1. Also, in most cases, **BF would often drop smoothly as more output tokens are generated**. Under the same task, when $C > 0$, different C mainly controls the starting point and the rate of decreasing, while in the end, they would converge to roughly the same point. When almost zero knowledge is provided ($C = 0$), the output will end much earlier compared to $C > 0$ cases. These findings also provide support that the future token generation is gradually becoming predictable and the model may have a certain generation plan to follow, resonating with recent observations in interpretability (Pal et al., 2023; Wu et al., 2024; Li et al., 2024a) and inference acceleration (Cai et al., 2024; Welleck et al., 2024). **A Matched-Length Control for CoT.** A natural concern is that CoT generations are longer, so their lower BF might simply reflect the general decline of BF over output position. To control for this, we compare BF at fixed truncated lengths on MMLU between reasoning-oriented models (DeepSeek-R1-Distill-Llama-8B/70B) and direct-answer instruct models (Llama-3-8B/70B-Instruct), following the same measurement protocol as

[7]See § D for full results across all models and tasks.

above. Each point on the x-axis corresponds to BF computed up to the same truncated length, enabling a fair matched-position comparison.

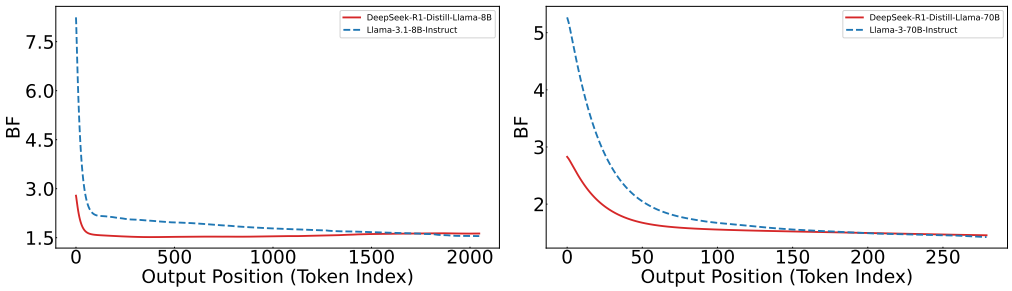

(a) Llama-3-8B (b) Llama-3-70B

Figure 4: **Matched-length BF comparison on MMLU.** At every truncated length, the reasoning-oriented models (DeepSeek-R1-Distill-Llama) exhibit lower BF than the direct-answer instruct models, including at the earliest matched positions.

As shown in Figure 4, the reasoning-oriented models exhibit consistently lower BF across all truncated positions, including the earliest generation stages. This suggests that their lower BF is not merely a byproduct of longer generations drifting into lower-BF regions, and provides a practical check that BF comparisons are robust to this length confound. We further examine potential confounds such as prompt likelihood and data contamination in § L, and find they do not fully account for the observed BF reductions.

4.2 Pareto Analysis of BF

How dominant is this alignment effect compared to other factors? Figure 5a offers a first look: the Base/Aligned BF ratio is consistently high ($\gg 1$) across diverse tasks and models, peaking at $10\times$ for Random Strings (task-wide) and appearing overall mildest for OLMo-2 (model-wide). To rigorously rank alignment against model size (S), generation (G), and prompt complexity (C), we perform a Pareto analysis (Figure 5) for Llama models. For each factor D_i, we define the unnormalized *Impact* $\tilde{I}(D_i)$ as the average absolute pairwise difference in BF when varying D_i while holding other dimensions constant:

$$\tilde{I}(D_i) = \frac{\sum_{d_i, d_j \in \text{Domain}(D_i), d_i \neq d_j} |\text{Avg}(\text{B}(\cdot|D_i = d_i)) - \text{Avg}(\text{B}(\cdot|D_i = d_j))|}{|\text{Domain}(D_i)| \times |\text{Domain}(D_i) - 1|}. \tag{9}$$

Then we normalize it as $I(D_i) = \frac{\tilde{I}(D_i)}{\sum_k \tilde{I}(D_k)}$.

The results crisply validate our intuition: **alignment tuning is the primary driver of BF reduction**. Across all tasks, it consistently crosses or approaches the 80% cumulative impact threshold, surpassing all other factors by a large margin.

Among the secondary factors, for tasks with richer inputs–such as MMLU (with more in-context examples) and BBCLatestNews (with more headlines)–prompt complexity C and model size S emerge as the next most impactful. Prompt complexity C has a noteworthy effect: contrary to intuition, more context provided in the prompt does not always reduce BF but can in fact increase it, potentially due to the cognitive burden of processing complex linguistic structures. A detailed case study and comprehensive task-wise BF results are presented in §§ E and F. In contrast, for open-ended tasks like Cognac and Story Generation, model generation G plays a more dominant role, particularly improvements from Llama-2 to Llama-3. This shift likely reflects gains from the use of larger, more diverse datasets in training (Dubey et al., 2024).

5 Low Branching Factor Explains Generative Stability and Commitment

Our analysis in § 4 established that BF declines over the generation process (§ 4.1) and is significantly lower in aligned models (§ 4.2). This structural concentration of probability mass provides a unified

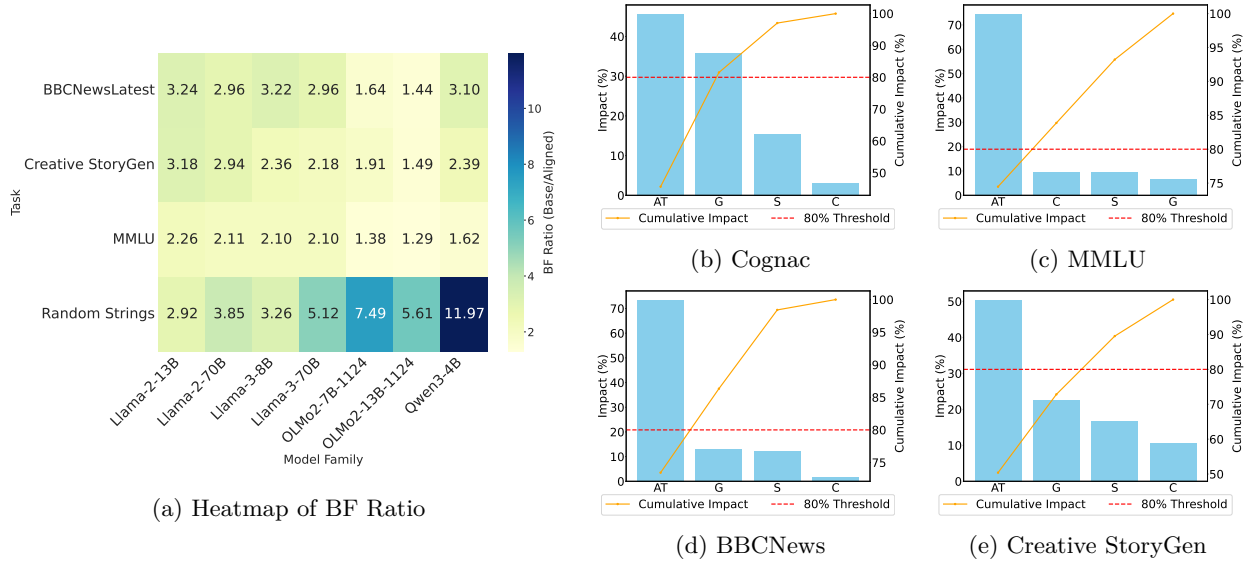

(a) Heatmap of BF Ratio (b) Cognac (c) MMLU (d) BBCNews (e) Creative StoryGen

Figure 5: **Attributing BF Reduction.** (a) Heatmap of average BF ratio (Base/Aligned) across tasks and models. The numbers indicate the average ratio over all constraint levels. Note that for OLMo-2, we follow the convention in (OLMo et al., 2024) and treat the DPO version as the aligned model. (b)-(e) Pareto Analysis of BF across various IFs. AT indicates whether the model is aligned. C denotes the prompt complexity. S refers to model size, and G refers to model generation.

probabilistic explanation for three distinct generative behaviors: the insensitivity of aligned models to decoding hyperparameters, their reduced variance in majority voting, and the high performance cost of late-stage exploration.

5.1 Insensitivity to Decoding Configurations

Model developers adopt different decoding strategies when reporting LLM capabilities (Touvron et al., 2023; Dubey et al., 2024; Yang et al., 2024; Guo et al., 2025). The effectiveness of strategies like nucleus sampling (p) and temperature sampling (T) relies on the assumption that a diverse set of plausible next tokens exists. However, our BF analysis suggests that for aligned models, the "plausible set" is much smaller. If this holds, we expect aligned models to be robust to decoding choices, as there are few alternatives for the decoding algorithm to select even at higher temperatures.

We verify this by benchmarking decoding methods on MMLU-STEM (Hendrycks et al., 2021), extending prior work (Song et al., 2024; Renze & Guven, 2024; Shi et al., 2024a) to the latest models including DeepSeek-distilled models (Guo et al., 2025), which would generate long CoT before the final answer.[8] Specifically, we evaluate model performance on MMLU-STEM (Hendrycks et al., 2021) under CoT prompting across different temperatures (T= 0.6/1.0) in temperature sampling and truncation thresholds (p=0.9/1.0) in nucleus sampling (Holtzman et al., 2020). Further implementation details can be found in § A.

As shown in Table 1, aligned models exhibit limited performance variation (typically $< 10\%$) even when shifting from greedy-like settings to high temperatures. In contrast, Base models, which maintain higher BF, show significant sensitivity (up to 31%) to decoding parameters. Notably, DeepSeek-distilled Llama-8B, which generates long CoT and thus maintains a consistently low BF throughout generation, exhibits the smallest relative performance changes among 8B models. This empirically supports that *low BF effectively nullifies the impact of sampling method choices.*

[8]For Llama-3 series models, in our prior study, we find there is only a minor performance difference between Llama-3 and Llama-3.x. We mainly use Llama-3 in this paper as it includes the most diverse model collection.

Models	Default (T=0.6, p=0.9)	T=0.6, p=1.0	T=1.0, p=0.9	Min (T=1.0, p=1.0)	$\frac{\text{Default}-\text{Min}}{\text{Default}}$%
Llama-3-70B-Instruct	78.50 (± 2.09)	77.60 (± 2.23)	77.50 (± 2.60)	75.90 (± 2.85)	3.31
Llama-3-70B	78.00 (± 3.52)	74.00 (± 3.80)	72.00 (± 4.38)	63.50 (± 5.02)	18.59
DeepSeek-R1-Distill-Llama-8B	66.30 (± 3.51)	65.70 (± 3.84)	62.70 (± 4.14)	59.70 (± 4.65)	9.95
Llama-3.1-8B-Instruct	63.00 (± 4.01)	61.50 (± 4.37)	57.50 (± 4.92)	50.50 (± 5.34)	19.84
Llama-3.1-8B	54.00 (± 4.61)	53.50 (± 4.92)	47.00 (± 5.21)	37.00 (± 5.48)	**31.48**

Table 1: **Experiment Results across decoding methods on STEM subset of MMLU.** We follow the common practice of using 5-shot CoT prompting. $\frac{\text{Default}-\text{Min}}{\text{Default}}$% indicates the maximum relative performance drop when deviating from the default decoding configuration.

Model	Maj@1 Std	Maj@3 Std	Maj@8 Std	Maj@16 Std	BF
DeepSeek-R1-Distill-Llama-70B	**14.34**	**8.29**	**4.99**	**3.21**	**1.23**
Llama-3-70B-Instruct	16.37	11.40	7.50	5.12	1.28
Llama-3-70B	27.78	19.53	13.22	9.23	1.31
DeepSeek-R1-Distill-Llama-8B	**27.10**	**20.91**	**13.93**	**9.14**	**1.23**
Llama-3.1-8B-Instruct	31.54	24.64	17.30	12.90	1.31
Llama-3.1-8B	36.41	29.78	20.43	14.05	1.35

Table 2: **Majority Voting@K standard deviation on MMLU-STEM with** 200 **samples.** We compute the standard deviation over 100 bootstrapping trials, each using 64 samples per instance. We set $T = 0.6, p = 0.9$ to match standard benchmarking settings, differing from $T = 1.0, p = 0.9$ setup in § 4. Lower temperature concentrates probability mass on fewer tokens, reducing BF and complicating direct comparisons. However, bootstrapping (100 runs) reveals minimal variability (≈ 0.01), confirming that the BF differences reported here remain significant. Consequently, BF remains a strong predictor of standard deviation.

5.2 Reduced Variance in Majority Voting

If aligned models have a restricted output space (low BF), this should also manifest as reduced variance across independent samples. We test this hypothesis by evaluating output variance on MMLU-STEM using 200 samples per model. We benchmark the standard deviation across Majority@K accuracy metrics ($K = 1, 3, 8, 16$) with $T = 0.6, p = 0.9$.

As detailed in Table 2, BF serves as a strong predictor of sampling consistency. The Long-CoT models (DeepSeek-R1-Distill), which generate significantly longer outputs and achieve the lowest global BF, consistently show the smallest performance variance. This confirms that the "stability" observed in decoding benchmarks is not an artifact of specific hyperparameters, but a fundamental property of the narrowed generation manifold.

5.3 Risks of Mid-Generation Forking

The stability provided by low BF suggests a strong commitment to a specific reasoning trajectory. Does this commitment imply that the model cannot effectively explore alternative paths once generation has begun? If BF reflects a semantic "lock-in," forcing the model to branch out (fork) at late, low-BF stages should disrupt coherence and degrade performance.

To examine this, we conduct a resampling experiment using DeepSeek-Distilled Llama-8B output samples. Procedurally, for a given position t: 1) Take the prefix $y_{<t}$ generated by the model. 2) Sample a new continuation $y'_{\geq t}$ from $P(\mathrm{Y}_{\geq t}|[x, y_{<t}]; \theta)$. 3) Evaluate the full sequence $[y_{<t}, y'_{\geq t}]$ on the task.

As shown in Figure 6, performance drops sharply when resampling occurs at a later, lower-BF position in the sequence. This suggests that aligned models are not just concentrating probability mass locally (reflects a "deeper commitment" to specific paths), but are actively locking into trajectories, making late-stage deviations more error-prone. In practice, this highlights a key application of BF: *parallel sampling should be applied early, while BF remains high*, to ensure meaningful diversity and avoid quality degradation.

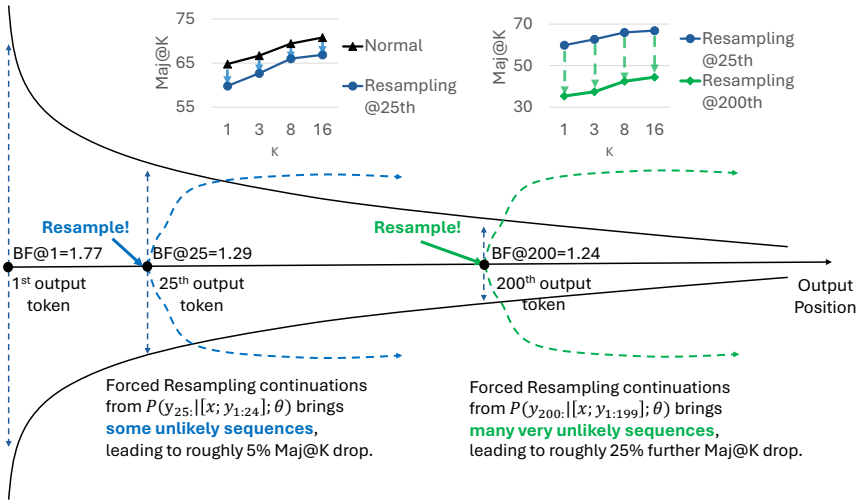

Figure 6: **Resampling from different output positions to assess the effect of interrupting BF reduction**. We resample new continuations at the 25th and 200th output token of DeepSeek-Distilled Llama-8B MMLU outputs. Results show substantial performance drops at both positions.

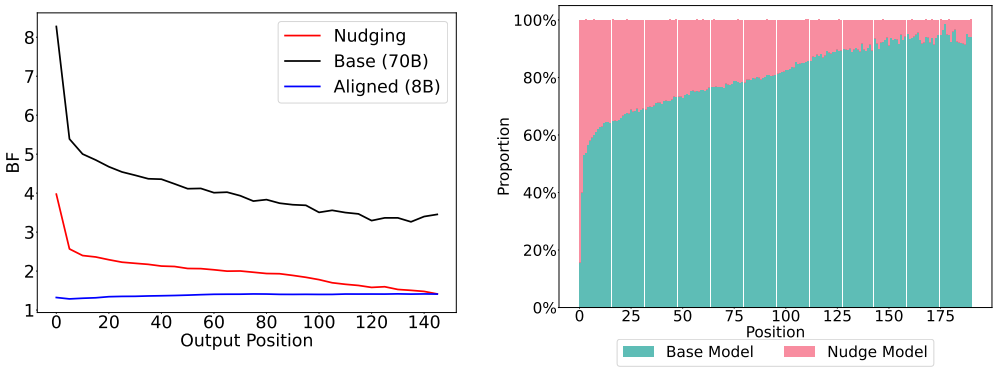

(a) Output BF Dynamics (b) Nudging Ratio Histogram

Figure 7: Nudging Experiments over Just-Eval-Instruct.

6 How does Alignment Tuning Impact BF?

Why does alignment tuning exert such a pronounced effect on BF? Building on the superficial alignment hypothesis (Zhou et al., 2024) ("*Alignment tuning might simply teach base LLMs to select a subdistribution of data formats for interacting with users.*") and recent tuning-free alignment work (Lin et al., 2023; Fei et al., 2024; Lake et al., 2025), we hypothesize base models already encode low-entropy conditional distributions. In this view, alignment tuning doesn't reshape generation from scratch, but instead nudge the model toward *stylistic tokens* (e.g., "Sure"), thereby narrowing the conditional distribution.

To test this hypothesis, we reproduce the nudging experiments (Fei et al., 2024), over Just-Eval-Instruct (Lin et al., 2023) and MMLU datasets. We employ Llama-3-70B for drafting most outputs. However, when the base model's Top-1 probability is low, we apply nudging by switching to Llama-3-8B-Instruct to generate a single word. Using a smaller aligned model to nudge a larger base model (70B) isolates the steering effect of the stylistic prefix itself, independent of the nudging model's raw capability. BF was computed as in prior experiments. The results, shown in Figure 7,[9] indicate that after most nudging occurs early in the generation process – indicating the prefix generated by the nudging model is of low probability. These observations collectively support our hypothesis. Considering that nudging not only reduces BF but also improves aligned model performance on these tasks (Fei et al., 2024), our results highlight the dual effect of alignment training: reducing BF while preserving or even enhancing task performance.

[9]We present results on Just-Eval-Instruct only for brevity. MMLU results are included in § I.

Which Training Stage Reduces BF Most? While our nudging analysis suggests alignment tuning narrows the distribution by nudging models toward stylistic tokens, it remains unclear which specific phase of the pipeline drives this reduction. Disentangling these effects is difficult because most model releases (e.g., Llama 3 (Dubey et al., 2024)) do not provide intermediate checkpoints, and modern post-training often employs iterative, interleaved schedules rather than discrete stages. However, the OLMo-2 suite (OLMo et al., 2024) releases intermediate checkpoints, enabling a preliminary stage-wise dissection. We measure BF changes across Supervised Fine-Tuning (SFT) and Direct Preference Optimization (DPO) (Rafailov et al., 2023) stages on the open-ended Creative StoryGen task. As shown in Figure 8, we observe distinct behaviors across model scales: for the 7B OLMo-2 model, SFT is the primary driver of BF reduction, causing a 42.3% drop compared with 20.5% for DPO, whereas for the 13B OLMo-2 model, the DPO stage contributes more significantly, with a 25.6% drop compared with 14.9% for the SFT stage. This divergence suggests that the impact of alignment tuning stages is not universal but sensitive to specific training recipes and model scales.

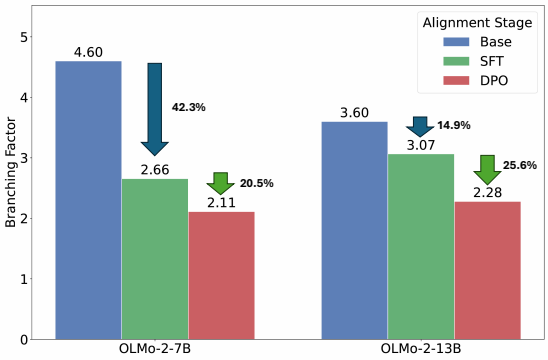

Figure 8: **Stage-wise Contribution to BF Reduction.** We analyze OLMo-2 models on the Creative StoryGen task.

Beyond OLMo-2: Other Post-Training Algorithms. The OLMo-2 checkpoints provide a clean stage-wise comparison, but they only cover the SFT and DPO stages. To broaden the picture, we next study a publicly released RLHF pipeline from RLHFlow (Dong et al., 2024) and OpenRLHF (Hu et al., 2024) collaboration, which includes checkpoints for SFT, DPO, PPO, and Iterative DPO variants. Because post-training recipes vary substantially across organizations (e.g., in data and training setup), we view this as a controlled case study rather than a universal ranking of algorithms. We evaluate all checkpoints on Creative StoryGen using the same setup as above.

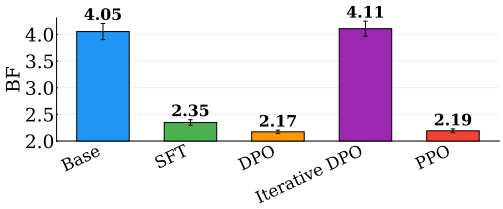

Figure 9: **BF across post-training algorithms.** Using checkpoints from an RLHFlow/OpenRLHF pipeline on Creative StoryGen, we find that SFT drives the largest BF drop, DPO and PPO yield similar further reductions, and Iterative DPO partially preserves distributional breadth.

As shown in Figure 9, SFT again accounts for the largest BF reduction (4.05 → 2.35), consistent with the OLMo-2 trend. DPO and PPO then produce very similar additional reductions (2.35 → 2.17 for DPO and 2.35 → 2.19 for PPO), suggesting that these two offline preference-optimization methods concentrate the distribution to a comparable extent beyond the SFT stage. Iterative DPO, however, avoids part of this shrinkage. A plausible explanation is that its more online training loop repeatedly refreshes the reference policy and collects preference signals from the model's updated outputs, which can expose the model to underrepresented regions of the solution space instead of reinforcing a fixed offline preference set. This interpretation is consistent with Wu et al. (2025b), who argue that offline reinforcement-style methods remain tightly tethered to their initial reference policy and therefore have limited ability to move beyond it.

7 Related Works

Uncertainty Quantification for LLM. Uncertainty quantification (UQ) for LLMs has gained significant attention due to its importance in real-world applications, particularly in high-stakes domains (Desai & Durrett, 2020; Jiang et al., 2021; Wang et al., 2022; Kadavath et al., 2022; Xiong et al., 2024; Ye et al., 2024; Gupta et al., 2024). Existing methods typically address closed-domain tasks such as classification and question-answering, where outputs are discrete and easier to assess. However, as Kuhn et al. (2023) note, these approaches often overlook challenges specific to open-ended generation, such as semantic equivalence across outputs. They introduce "semantic entropy" to quantify uncertainty in LLM output space by first clustering the sampled output and then quantifying uncertainty over cluster distribution. This method empirically works well in hallucination detection (Farquhar et al., 2024). In this paper, we focus on investigating the

probability concentration phenomenon for LLMs. We introduce BF to quantify this concentration, which applies broadly across tasks without imposing strong assumptions on output categories.

Reduced Diversity in Aligned Models. Recent studies have consistently shown that alignment tuning reduces output diversity in language models (Perez et al., 2022; Padmakumar & He, 2024; Chakrabarty et al., 2024; Tian et al., 2024; Kirk et al., 2024; Lu et al., 2025; Lake et al., 2025; West & Potts, 2025). Mechanistically, Lake et al. (2025) observe that alignment suppresses diversity by aggregating information into longer, standardized responses, though they argue this preserves useful base model behaviors. Our work builds on this inquiry by connecting reduced diversity with related observations on diminished randomness and robustness in aligned models (Saparov & He, 2023; Song et al., 2024; Renze & Guven, 2024; Bigelow et al., 2024), and proposes a unifying explanation: increased probability concentration. Traditional diversity metrics such as n-gram lexical diversity (Li et al., 2016) are sensitive to vocabulary size and output length (Liu et al., 2022; Tevet & Berant, 2021; Guo et al., 2024; Kirk et al., 2024) and cannot work well with most recent long CoT models. In § K, we demonstrate that lexical diversity poorly correlates with BF and fails to robustly measure generation concentration.

Our work also resonates with information density research in cognitive science and linguistic theories, and we present a short discussion in § J.

8 Discussion

Practical Implications. A key practical implication of our findings is that reduced BF neglects alternative generations and forking. Consequently, simply tweaking decoding parameters (e.g., temperature), is unlikely to restore diversity without severely degrading quality (Renze & Guven, 2024). Our work offers a clear explanation for why this occurs, particularly for methods like beam search. The resampling experiment in § 5.3 provides direct evidence that for low-BF models, off-path trajectories are not just less probable but often of lower quality. With little probability mass distributed among alternative paths, beam search has few viable options to explore, yielding diminishing returns. This suggests that efforts to mitigate diversity loss should target the training process itself – a more promising, albeit challenging, direction. Future work could involve curating more diverse alignment data or designing novel training objectives that balance instruction-following with distributional diversity (Wang et al., 2024; Kwon et al., 2024; Lanchantin et al., 2025; Chung et al., 2025). System-level interventions (e.g., model collaboration) also present a viable path forward (Fei et al., 2024; Lu et al., 2024; Venkatraman et al., 2025; Ismayilzada et al., 2025). While our paper's primary contribution is diagnostic, we believe this foundational understanding is a necessary prerequisite for developing such effective countermeasures.

That said, the above discussion applies primarily to settings where output diversity is valued, such as creative generation, open-ended dialogue, and exploratory reasoning. For tasks with unique correct answers (e.g., arithmetic, factual retrieval), low BF might in fact be desirable – it might reflect the model concentrating probability mass on the correct output, and alignment-induced BF reduction can be beneficial.

Societal Homogeneity Bias of Alignment Tuning. Our work identifies a key dynamic in modern LLMs: alignment tuning significantly reduces the Branching Factor (BF), leading to more homogenized and predictable outputs. While this can be beneficial, it also carries potential negative societal impacts. In applications such as automated content generation, creative writing, or decision-support systems (Padmakumar & He, 2024; Sorensen et al., 2024; Wu et al., 2025a; Murthy et al., 2025; Rodemann et al., 2025; Ashkinaze et al., 2025; Lake et al., 2025), this reduction in diversity could inadvertently reinforce social biases, stifle creativity, and limit the exploration of novel ideas. Rodemann et al. (2025) further argue that empirical alignment, relying on limited and potentially biased human feedback, creates selectional bias that fails to capture the full spectrum of human values. We believe that formally understanding and quantifying the mechanisms of probability concentration, as we do in this paper, is a critical and necessary first step toward developing alignment techniques that mitigate these risks and foster models that are not only helpful and harmless but also diverse and robust.

9 Limitations

BF is a First-Moment Summary. By definition, BF captures the exponentiated length-averaged entropy – a single scalar. Like any such summary, it can obscure higher-order structural properties of the generative distribution. Consider a stylized example with sequences of length $N = 2$ over vocabulary a, b, c, d. DISTRIBUTION A (uniform branching): $P(Y_1 = a) = P(Y_1 = b) = 1/2$, $P(Y_2 = c \mid Y_1) = P(Y_2 = d \mid Y_1) = 1/2$ regardless of Y_1. DISTRIBUTION B (front-loaded branching): $P(Y_1)$ is uniform over all four tokens, while $P(Y_2 \mid Y_1)$ is deterministic. Both distributions yield $\tilde{H}(Y_{1:2}) = 2 \ln 2$ and hence $BF = 2$, yet they correspond to qualitatively different trees. Nonetheless, BF is designed to answer a specific question — how concentrated is the generation process on average – and practitioners who require finer-grained characterization of the tree topology should complement BF with positional or higher-order analyses.

Estimation Variance at Short Horizons. Our efficient BF estimator relies on the asymptotic convergence between length-averaged NLL and realized entropy (Theorem 3.1), a gap that shrinks as the sequence length N grows but can be non-negligible for short sequences. To address this, we adopt a hybrid strategy (Equation (8)): for sequences shorter than a threshold L_τ, we compute the exact realized entropy via full vocabulary summation, resorting to the NLL approximation only for longer sequences where it is both accurate and computationally necessary. Figures 2(c) and 2(d) empirically validate this design: the standard deviation of the length-averaged NLL estimator diminishes rapidly, falling to practical levels within roughly 20 tokens. These observations provide concrete guidance for practitioners – exact entropy computation is feasible and recommended for short outputs (we recommend choosing a L_τ between 20 and 50), while the NLL proxy can be safely adopted beyond this early regime.

References

Joshua Ashkinaze, Julia Mendelsohn, Li Qiwei, Ceren Budak, and Eric Gilbert. How ai ideas affect the creativity, diversity, and evolution of human ideas: evidence from a large, dynamic experiment. In *Proceedings of the ACM Collective Intelligence Conference*, pp. 198–213, 2025.

Yuntao Bai, Andy Jones, Kamal Ndousse, Amanda Askell, Anna Chen, Nova DasSarma, Dawn Drain, Stanislav Fort, Deep Ganguli, Tom Henighan, et al. Training a helpful and harmless assistant with reinforcement learning from human feedback. *arXiv preprint arXiv:2204.05862*, 2022.

Eric J Bigelow, Ekdeep Singh Lubana, Robert P. Dick, Hidenori Tanaka, and Tomer Ullman. In-context learning dynamics with random binary sequences. In *The Twelfth International Conference on Learning Representations*, 2024. URL `https://openreview.net/forum?id=62K7mALO2q`.

Tianle Cai, Yuhong Li, Zhengyang Geng, Hongwu Peng, Jason D. Lee, Deming Chen, and Tri Dao. Medusa: Simple LLM inference acceleration framework with multiple decoding heads. In *Forty-first International Conference on Machine Learning*, 2024. URL `https://openreview.net/forum?id=PEpbUobfJv`.

Tuhin Chakrabarty, Philippe Laban, Divyansh Agarwal, Smaranda Muresan, and Chien-Sheng Wu. Art or artifice? large language models and the false promise of creativity. In *Proceedings of the CHI Conference on Human Factors in Computing Systems*, pp. 1–34, 2024.

Howard Chen, Huihan Li, Danqi Chen, and Karthik Narasimhan. Cognac: Controllable text generation with language constraints. In *arXiv*, 2022.

Daixuan Cheng, Shaohan Huang, Xuekai Zhu, Bo Dai, Wayne Xin Zhao, Zhenliang Zhang, and Furu Wei. Reasoning with exploration: An entropy perspective. *arXiv preprint arXiv:2506.14758*, 2025.

John Joon Young Chung, Vishakh Padmakumar, Melissa Roemmele, Yuqian Sun, and Max Kreminski. Modifying large language model post-training for diverse creative writing. *arXiv preprint arXiv:2503.17126*, 2025.

Ganqu Cui, Yuchen Zhang, Jiacheng Chen, Lifan Yuan, Zhi Wang, Yuxin Zuo, Haozhan Li, Yuchen Fan, Huayu Chen, Weize Chen, et al. The entropy mechanism of reinforcement learning for reasoning language models. *arXiv preprint arXiv:2505.22617*, 2025.

Shrey Desai and Greg Durrett. Calibration of pre-trained transformers. *arXiv preprint arXiv:2003.07892*, 2020.

Hanze Dong, Wei Xiong, Bo Pang, Haoxiang Wang, Han Zhao, Yingbo Zhou, Nan Jiang, Doyen Sahoo, Caiming Xiong, and Tong Zhang. Rlhf workflow: From reward modeling to online rlhf. *Transactions on Machine Learning Research*, 2024.

Abhimanyu Dubey, Abhinav Jauhri, Abhinav Pandey, Abhishek Kadian, Ahmad Al-Dahle, Aiesha Letman, Akhil Mathur, Alan Schelten, Amy Yang, Angela Fan, et al. The llama 3 herd of models. *arXiv preprint arXiv:2407.21783*, 2024.

Ondřej Dušek, Jekaterina Novikova, and Verena Rieser. Evaluating the state-of-the-art of end-to-end natural language generation: The e2e nlg challenge. *Computer Speech & Language*, 59:123–156, 2020.

Sebastian Farquhar, Jannik Kossen, Lorenz Kuhn, and Yarin Gal. Detecting hallucinations in large language models using semantic entropy. *Nature*, 630(8017):625–630, 2024.

Yu Fei, Yasaman Razeghi, and Sameer Singh. Nudging: Inference-time alignment via model collaboration. *arXiv preprint arXiv:2410.09300*, 2024.

Dmitriy Genzel and Eugene Charniak. Entropy rate constancy in text. In *Proceedings of the 40th annual meeting of the Association for Computational Linguistics*, pp. 199–206, 2002.

Daya Guo, Dejian Yang, Haowei Zhang, Junxiao Song, Ruoyu Zhang, Runxin Xu, Qihao Zhu, Shirong Ma, Peiyi Wang, Xiao Bi, et al. Deepseek-r1: Incentivizing reasoning capability in llms via reinforcement learning. *arXiv preprint arXiv:2501.12948*, 2025.

Yanzhu Guo, Guokan Shang, and Chloé Clavel. Benchmarking linguistic diversity of large language models. *arXiv preprint arXiv:2412.10271*, 2024.

Neha Gupta, Harikrishna Narasimhan, Wittawat Jitkrittum, Ankit Singh Rawat, Aditya Krishna Menon, and Sanjiv Kumar. Language model cascades: Token-level uncertainty and beyond. In *The Twelfth International Conference on Learning Representations*, 2024.

Shibo Hao, Yi Gu, Haodi Ma, Joshua Hong, Zhen Wang, Daisy Wang, and Zhiting Hu. Reasoning with language model is planning with world model. In *Proceedings of the 2023 Conference on Empirical Methods in Natural Language Processing*, pp. 8154–8173, 2023.

Dan Hendrycks, Collin Burns, Steven Basart, Andy Zou, Mantas Mazeika, Dawn Song, and Jacob Steinhardt. Measuring massive multitask language understanding. In *International Conference on Learning Representations*, 2021. URL `https://openreview.net/forum?id=d7KBjmI3GmQ`.

John Hewitt, Christopher D Manning, and Percy Liang. Truncation sampling as language model desmoothing. In *Findings of the Association for Computational Linguistics: EMNLP 2022*, pp. 3414–3427, 2022.

Ari Holtzman, Jan Buys, Li Du, Maxwell Forbes, and Yejin Choi. The curious case of neural text degeneration. In *International Conference on Learning Representations*, 2020. URL `https://openreview.net/forum?id=rygGQyrFvH`.

Jian Hu, Xibin Wu, Zilin Zhu, Xianyu, Weixun Wang, Dehao Zhang, and Yu Cao. Openrlhf: An easy-to-use, scalable and high-performance rlhf framework. *arXiv preprint arXiv:2405.11143*, 2024.

Mete Ismayilzada, Antonio Laverghetta Jr, Simone A Luchini, Reet Patel, Antoine Bosselut, Lonneke van der Plas, and Roger Beaty. Creative preference optimization. *arXiv preprint arXiv:2505.14442*, 2025.

T Jaeger and Roger Levy. Speakers optimize information density through syntactic reduction. *Advances in neural information processing systems*, 19, 2006.

Zhengbao Jiang, Jun Araki, Haibo Ding, and Graham Neubig. How can we know when language models know? on the calibration of language models for question answering. *Transactions of the Association for Computational Linguistics*, 9:962–977, 2021.

Daniel Jurafsky and James H. Martin. *Speech and Language Processing: An Introduction to Natural Language Processing, Computational Linguistics, and Speech Recognition, with Language Models*. 3rd edition, 2025. URL `https://web.stanford.edu/~jurafsky/slp3/`. Online manuscript released August 24, 2025.

Saurav Kadavath, Tom Conerly, Amanda Askell, Tom Henighan, Dawn Drain, Ethan Perez, Nicholas Schiefer, Zac Hatfield-Dodds, Nova DasSarma, Eli Tran-Johnson, et al. Language models (mostly) know what they know. *arXiv preprint arXiv:2207.05221*, 2022.

Robert Kirk, Ishita Mediratta, Christoforos Nalmpantis, Jelena Luketina, Eric Hambro, Edward Grefenstette, and Roberta Raileanu. Understanding the effects of RLHF on LLM generalisation and diversity. In *The Twelfth International Conference on Learning Representations*, 2024. URL `https://openreview.net/forum?id=PXD3FAVHJT`.

Lorenz Kuhn, Yarin Gal, and Sebastian Farquhar. Semantic uncertainty: Linguistic invariances for uncertainty estimation in natural language generation. In *The Eleventh International Conference on Learning Representations*, 2023.

Oh Joon Kwon, Daiki E Matsunaga, and Kee-Eung Kim. Gdpo: Learning to directly align language models with diversity using gflownets. *arXiv preprint arXiv:2410.15096*, 2024.

Thom Lake, Eunsol Choi, and Greg Durrett. From distributional to overton pluralism: Investigating large language model alignment. In *Proceedings of the 2025 Conference of the Nations of the Americas Chapter of the Association for Computational Linguistics: Human Language Technologies (Volume 1: Long Papers)*, pp. 6794–6814, 2025.

Jack Lanchantin, Angelica Chen, Shehzaad Dhuliawala, Ping Yu, Jason Weston, Sainbayar Sukhbaatar, and Ilia Kulikov. Diverse preference optimization. *arXiv preprint arXiv:2501.18101*, 2025.

Roger Levy. Expectation-based syntactic comprehension. *Cognition*, 106(3):1126–1177, 2008.

Jiwei Li, Michel Galley, Chris Brockett, Jianfeng Gao, and William B Dolan. A diversity-promoting objective function for neural conversation models. In *Proceedings of the 2016 Conference of the North American Chapter of the Association for Computational Linguistics: Human Language Technologies*, pp. 110–119, 2016.

Margaret Li, Weijia Shi, Artidoro Pagnoni, Peter West, and Ari Holtzman. Predicting vs. acting: A trade-off between world modeling & agent modeling. *arXiv preprint arXiv:2407.02446*, 2024a.

Yucheng Li, Frank Guerin, and Chenghua Lin. Latesteval: Addressing data contamination in language model evaluation through dynamic and time-sensitive test construction. In *Proceedings of the AAAI Conference on Artificial Intelligence*, volume 38, pp. 18600–18607, 2024b.

Bill Yuchen Lin, Abhilasha Ravichander, Ximing Lu, Nouha Dziri, Melanie Sclar, Khyathi Chandu, Chandra Bhagavatula, and Yejin Choi. The unlocking spell on base llms: Rethinking alignment via in-context learning. In *The Twelfth International Conference on Learning Representations*, 2023.

Siyang Liu, Sahand Sabour, Yinhe Zheng, Pei Ke, Xiaoyan Zhu, and Minlie Huang. Rethinking and refining the distinct metric. In Smaranda Muresan, Preslav Nakov, and Aline Villavicencio (eds.), *Proceedings of the 60th Annual Meeting of the Association for Computational Linguistics (Volume 2: Short Papers)*, pp. 762–770, Dublin, Ireland, May 2022. Association for Computational Linguistics. doi: 10.18653/v1/2022.acl-short.86. URL `https://aclanthology.org/2022.acl-short.86/`.

Li-Chun Lu, Shou-Jen Chen, Tsung-Min Pai, Chan-Hung Yu, Hung-yi Lee, and Shao-Hua Sun. Llm discussion: Enhancing the creativity of large language models via discussion framework and role-play. In *First Conference on Language Modeling*, 2024.

Ximing Lu, Melanie Sclar, Skyler Hallinan, Niloofar Mireshghallah, Jiacheng Liu, Seungju Han, Allyson Ettinger, Liwei Jiang, Khyathi Chandu, Nouha Dziri, and Yejin Choi. AI as humanity's salieri: Quantifying linguistic creativity of language models via systematic attribution of machine text against web text. In

The Thirteenth International Conference on Learning Representations, 2025. URL https://openreview.net/forum?id=ilOEOIqolQ.

Kyle Mahowald, Evelina Fedorenko, Steven T Piantadosi, and Edward Gibson. Info/information theory: Speakers choose shorter words in predictive contexts. *Cognition*, 126(2):313–318, 2013.

Clara Meister, Tiago Pimentel, Patrick Haller, Lena Jäger, Ryan Cotterell, and Roger Levy. Revisiting the uniform information density hypothesis. *arXiv preprint arXiv:2109.11635*, 2021.

William Merrill and Ashish Sabharwal. The parallelism tradeoff: Limitations of log-precision transformers. *Transactions of the Association for Computational Linguistics*, 11:531–545, 2023.

George A Miller. Wordnet: a lexical database for english. *Communications of the ACM*, 38(11):39–41, 1995.

Avinash Mudireddy, Tyler Bell, and Raghu Mudumbai. Slaves to the law of large numbers: An asymptotic equipartition property for perplexity in generative language models. *arXiv preprint arXiv:2405.13798*, 2024.

Sonia Krishna Murthy, Tomer Ullman, and Jennifer Hu. One fish, two fish, but not the whole sea: Alignment reduces language models' conceptual diversity. In Luis Chiruzzo, Alan Ritter, and Lu Wang (eds.), *Proceedings of the 2025 Conference of the Nations of the Americas Chapter of the Association for Computational Linguistics: Human Language Technologies (Volume 1: Long Papers)*, pp. 11241–11258, Albuquerque, New Mexico, April 2025. Association for Computational Linguistics. ISBN 979-8-89176-189-6. doi: 10.18653/v1/2025.naacl-long.561. URL https://aclanthology.org/2025.naacl-long.561/.

Shashi Narayan, Shay B Cohen, and Mirella Lapata. Don't give me the details, just the summary! topic-aware convolutional neural networks for extreme summarization. In *Proceedings of the 2018 Conference on Empirical Methods in Natural Language Processing*, pp. 1797–1807, 2018.

Brendan O'Connor. Perplexity as branching factor as shannon diversity index, 2013. URL https://brenocon.com/blog/2013/01/perplexity-as-branching-factor-as-shannon-diversity-index/. Accessed: 2024-09-28.

Team OLMo, Pete Walsh, Luca Soldaini, Dirk Groeneveld, Kyle Lo, Shane Arora, Akshita Bhagia, Yuling Gu, Shengyi Huang, Matt Jordan, et al. 2 olmo 2 furious. *arXiv preprint arXiv:2501.00656*, 2024.

Long Ouyang, Jeffrey Wu, Xu Jiang, Diogo Almeida, Carroll Wainwright, Pamela Mishkin, Chong Zhang, Sandhini Agarwal, Katarina Slama, Alex Ray, et al. Training language models to follow instructions with human feedback. *Advances in neural information processing systems*, 35:27730–27744, 2022.

Vishakh Padmakumar and He He. Does writing with language models reduce content diversity? In *The Twelfth International Conference on Learning Representations*, 2024. URL https://openreview.net/forum?id=Feiz5HtCD0.

Koyena Pal, Jiuding Sun, Andrew Yuan, Byron C Wallace, and David Bau. Future lens: Anticipating subsequent tokens from a single hidden state. In *Proceedings of the 27th Conference on Computational Natural Language Learning (CoNLL)*, pp. 548–560, 2023.

Ethan Perez, Saffron Huang, Francis Song, Trevor Cai, Roman Ring, John Aslanides, Amelia Glaese, Nat McAleese, and Geoffrey Irving. Red teaming language models with language models. In *Proceedings of the 2022 Conference on Empirical Methods in Natural Language Processing*, pp. 3419–3448, 2022.

Team Qwen. Qwen3 technical report, 2025. URL https://arxiv.org/abs/2505.09388.

Rafael Rafailov, Archit Sharma, Eric Mitchell, Christopher D Manning, Stefano Ermon, and Chelsea Finn. Direct preference optimization: Your language model is secretly a reward model. *Advances in neural information processing systems*, 36:53728–53741, 2023.

Matthew Renze and Erhan Guven. The effect of sampling temperature on problem solving in large language models. *arXiv preprint arXiv:2402.05201*, 2024.

Julian Rodemann, Esteban Garces Arias, Christoph Luther, Christoph Jansen, and Thomas Augustin. A statistical case against empirical human-ai alignment. *arXiv preprint arXiv:2502.14581*, 2025.

Abulhair Saparov and He He. Language models are greedy reasoners: A systematic formal analysis of chain-of-thought. In *The Eleventh International Conference on Learning Representations*, 2023. URL `https://openreview.net/forum?id=qFVVBzXxR2V`.

Claude E Shannon. A mathematical theory of communication. *The Bell system technical journal*, 27(3): 379–423, 1948.

Chufan Shi, Haoran Yang, Deng Cai, Zhisong Zhang, Yifan Wang, Yujiu Yang, and Wai Lam. A thorough examination of decoding methods in the era of llms. In *Proceedings of the 2024 Conference on Empirical Methods in Natural Language Processing*, pp. 8601–8629, 2024a.

Weijia Shi, Anirudh Ajith, Mengzhou Xia, Yangsibo Huang, Daogao Liu, Terra Blevins, Danqi Chen, and Luke Zettlemoyer. Detecting pretraining data from large language models. In *The Twelfth International Conference on Learning Representations*, 2024b.

Shivalika Singh, Freddie Vargus, Daniel D'souza, Börje Karlsson, Abinaya Mahendiran, Wei-Yin Ko, Herumb Shandilya, Jay Patel, Deividas Mataciunas, Laura O'Mahony, et al. Aya dataset: An open-access collection for multilingual instruction tuning. In *Proceedings of the 62nd Annual Meeting of the Association for Computational Linguistics (Volume 1: Long Papers)*, pp. 11521–11567, 2024.

Yifan Song, Guoyin Wang, Sujian Li, and Bill Yuchen Lin. The good, the bad, and the greedy: Evaluation of llms should not ignore non-determinism. *arXiv preprint arXiv:2407.10457*, 2024.

Taylor Sorensen, Jared Moore, Jillian Fisher, Mitchell Gordon, Niloofar Mireshghallah, Christopher Michael Rytting, Andre Ye, Liwei Jiang, Ximing Lu, Nouha Dziri, et al. Position: a roadmap to pluralistic alignment. In *Proceedings of the 41st International Conference on Machine Learning*, pp. 46280–46302, 2024.

Guy Tevet and Jonathan Berant. Evaluating the evaluation of diversity in natural language generation. In *Proceedings of the 16th Conference of the European Chapter of the Association for Computational Linguistics: Main Volume*, pp. 326–346, 2021.

Yufei Tian, Tenghao Huang, Miri Liu, Derek Jiang, Alexander Spangher, Muhao Chen, Jonathan May, and Nanyun Peng. Are large language models capable of generating human-level narratives? In *EMNLP*, 2024.

Hugo Touvron, Louis Martin, Kevin Stone, Peter Albert, Amjad Almahairi, Yasmine Babaei, Nikolay Bashlykov, Soumya Batra, Prajjwal Bhargava, Shruti Bhosale, et al. Llama 2: Open foundation and fine-tuned chat models. *arXiv preprint arXiv:2307.09288*, 2023.

Saranya Venkatraman, Nafis Irtiza Tripto, and Dongwon Lee. Collabstory: Multi-llm collaborative story generation and authorship analysis. In *Findings of the Association for Computational Linguistics: NAACL 2025*, pp. 3665–3679, 2025.

Vivek Verma, Nicholas Tomlin, and Dan Klein. Revisiting entropy rate constancy in text. In *Findings of the Association for Computational Linguistics: EMNLP 2023*, pp. 15537–15549, 2023.

Ziyu Wan, Xidong Feng, Muning Wen, Stephen Marcus McAleer, Ying Wen, Weinan Zhang, and Jun Wang. Alphazero-like tree-search can guide large language model decoding and training. In *Forty-first International Conference on Machine Learning*, 2024.

Chaoqi Wang, Yibo Jiang, Chenghao Yang, Han Liu, and Yuxin Chen. Beyond reverse kl: Generalizing direct preference optimization with diverse divergence constraints. In *The Twelfth International Conference on Learning Representations*, 2024.

Shenzhi Wang, Le Yu, Chang Gao, Chujie Zheng, Shixuan Liu, Rui Lu, Kai Dang, Xionghui Chen, Jianxin Yang, Zhenru Zhang, et al. Beyond the 80/20 rule: High-entropy minority tokens drive effective reinforcement learning for llm reasoning. *arXiv preprint arXiv:2506.01939*, 2025.

Yuxia Wang, Daniel Beck, Timothy Baldwin, and Karin Verspoor. Uncertainty estimation and reduction of pre-trained models for text regression. *Transactions of the Association for Computational Linguistics*, 10: 680–696, 2022.

Jason Wei, Xuezhi Wang, Dale Schuurmans, Maarten Bosma, Fei Xia, Ed Chi, Quoc V Le, Denny Zhou, et al. Chain-of-thought prompting elicits reasoning in large language models. In *NeurIPS*, 2022.

Sean Welleck, Amanda Bertsch, Matthew Finlayson, Hailey Schoelkopf, Alex Xie, Graham Neubig, Ilia Kulikov, and Zaid Harchaoui. From decoding to meta-generation: Inference-time algorithms for large language models. *Transactions on Machine Learning Research*, 2024. ISSN 2835-8856. URL `https://openreview.net/forum?id=eskQMcIbMS`. Survey Certification.

Peter West and Christopher Potts. Base models beat aligned models at randomness and creativity. *arXiv preprint arXiv:2505.00047*, 2025.

Fan Wu, Emily Black, and Varun Chandrasekaran. Generative monoculture in large language models. In *The Thirteenth International Conference on Learning Representations*, 2025a. URL `https://openreview.net/forum?id=yZ7sn9pyqb`.

Fang Wu, Weihao Xuan, Ximing Lu, Zaid Harchaoui, and Yejin Choi. The invisible leash: Why rlvr may not escape its origin. *arXiv preprint arXiv:2507.14843*, 2025b.

Wilson Wu, John X Morris, and Lionel Levine. Do language models plan ahead for future tokens? In *The First Conference on Language Modeling*, 2024.

Miao Xiong, Zhiyuan Hu, Xinyang Lu, YIFEI LI, Jie Fu, Junxian He, and Bryan Hooi. Can LLMs express their uncertainty? an empirical evaluation of confidence elicitation in LLMs. In *The Twelfth International Conference on Learning Representations*, 2024. URL `https://openreview.net/forum?id=gjeQKFxFpZ`.

An Yang, Baosong Yang, Binyuan Hui, Bo Zheng, Bowen Yu, Chang Zhou, Chengpeng Li, Chengyuan Li, Dayiheng Liu, Fei Huang, et al. Qwen2 technical report. *arXiv preprint arXiv:2407.10671*, 2024.

Shunyu Yao, Dian Yu, Jeffrey Zhao, Izhak Shafran, Tom Griffiths, Yuan Cao, and Karthik Narasimhan. Tree of thoughts: Deliberate problem solving with large language models. *Advances in neural information processing systems*, 36:11809–11822, 2023.

Fanghua Ye, Mingming Yang, Jianhui Pang, Longyue Wang, Derek F Wong, Emine Yilmaz, Shuming Shi, and Zhaopeng Tu. Benchmarking llms via uncertainty quantification. *arXiv preprint arXiv:2401.12794*, 2024.

Chunting Zhou, Pengfei Liu, Puxin Xu, Srinivasan Iyer, Jiao Sun, Yuning Mao, Xuezhe Ma, Avia Efrat, Ping Yu, Lili Yu, et al. Lima: Less is more for alignment. *Advances in Neural Information Processing Systems*, 36, 2024.

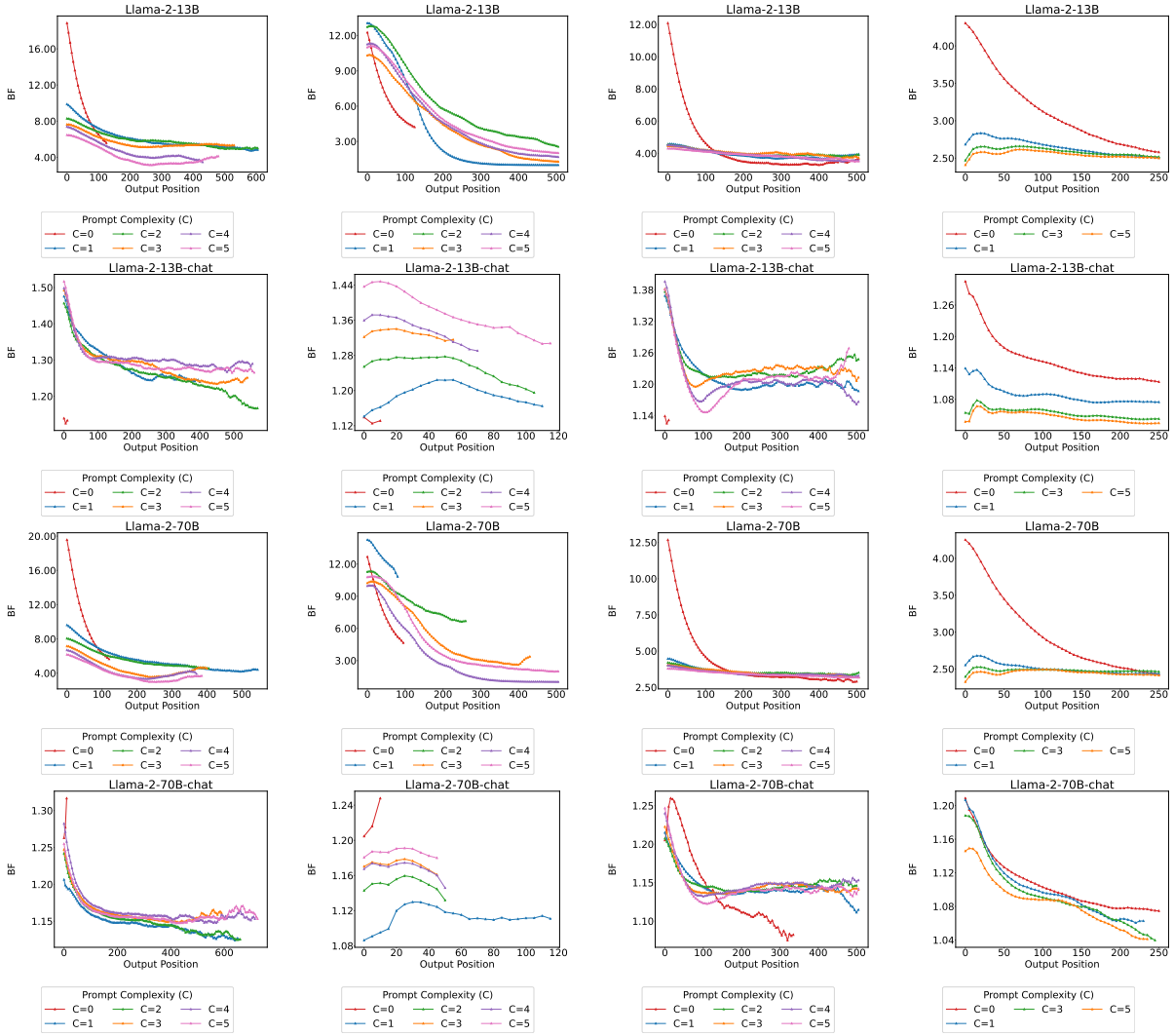

Figure 10: **BF Output Dynamic for Llama-2-families.** For better visualization, we compute the exponential moving averaged values of perplexity with the smoothing factor set as 0.1.

A Case Study Implementation Details

We use the scripts in Qwen-2.5-Math (Yang et al., 2024) for standard reasoning benchmarks.[10] We sample 200 examples from MMLU-STEM and compute the performance numbers under 64 trials and report the average performance.

B Dataset-Specific Processing

For all datasets we used in the paper, we carefully controlled whether the prompt length and expected output length would exceed the model's maximum length.

MMLU (Hendrycks et al., 2021) is a widely-used multiple-choice reasoning question. Unless otherwise explained, we use the full test set of MMLU to avoid potential contamination, following benchmarking settings reported in most LLM technical reports(Touvron et al., 2023; Dubey et al., 2024; Guo et al., 2025).

[10] `https://github.com/QwenLM/Qwen2.5-Math/tree/main`

We formulate prompt complexity C as the number of in-context samples. For example, $C = 1$ means we only add one in-context sample. For prompting setup and postprocessing details, we follow the standard implementation in Qwen-2.5-Math (Yang et al., 2024).

Cognac (Chen et al., 2022) is a controlled generation task requiring language model *not* to generate specified banned words provided in the prompt. We use the WordNet subset (Miller, 1995) of Cognac as this is the only released setting in Cognac paper, where the topic is a root node and the constraint is defined as a subtree. We sampled 200 instances using the provided data generation codes in our experiments. To ensure most model generations ended properly in the decoding process, we relax the constraint of maximum decoded tokens T from 60 to 512. We use the same prompt templates following their Github repo.[11]

Creative Story Generation (Chakrabarty et al., 2024) provides the plots and story continuation from both machine and human. We adopt the provided 11 human-written story plots in the original dataset as the prompt. In this task, we set the maximum token $T = 1024$ to ensure the continued story written by LLM can have a proper ending. We formulate prompt complexity C as providing $C \times 25$ words in the plot.

Random Strings Similar to Bigelow et al. (2024), we sample 200 random strings with length $L \sim U(256, 512)$ from the tokenizer vocabulary as the prompt. Prompt complexity C is formulated by providing $C \times 15$ tokens in the prompt, ensuring each article contains at least 100 tokens.

BBCLatestNews (Li et al., 2024b) is a news collection dataset aims at collecting news that is beyond the time cut for training LLMs. Unlike creative story plots, news articles are typically more structured and organized, although headlines can still be surprising. We select news articles from January to July 2024 to minimize data contamination, as the Llama models have a knowledge cut-off in late 2023. We formulate prompt complexity C as providing $C \times 15$ words in the prompt.

C Entropy Underestimation via Monte Carlo Sampling

To demonstrate the limitations of Monte Carlo (MC) sampling for entropy estimation in long sequences, we conducted an empirical study. We prompted Llama-3-8B-Instruct with 5-shot CoT examples from the MMLU dataset. We then estimated the entropy of its generated responses using a varying number of MC samples: $M \in \{4, 8, 16, 32, 64\}$.

As illustrated in Figure 12, the estimated entropy consistently increases with the number of samples. This trend confirms that MC estimation with a small sample size systematically **underestimates** the true entropy because it fails to capture the long tail of the full probability distribution. While increasing the sample count mitigates this bias, it does so at a significant computational cost. In contrast, Theorem 3.1 allows us to use the negative log-likelihood (NLL) of a single typical sequence for a more efficient and accurate estimation.

D Full BF Output Dynamics Investigation

Here we present full task-wise and model-wise BF output dynamic for Llama-2 in Figure 10 and Llama-3 in Figure 11. We can observe the trends as in § 4.1: ① **The average BF for the base model** (≈ 12) **is roughly ten times higher than the aligned model** (≈ 1.2). ② **BF would often drop smoothly as more output tokens are generated**.

E Curious Case of Prompt Complexity

Intuitively, greater prompt specificity (larger C) reduces BF by narrowing the model's output space through more informative context. However, our experimental results reveal task-varied effects. As illustrated in Figure 13 for the Cognac task, greater prompt complexity can *increase* BF–potentially due to the cognitive burden of processing negation or complex linguistic structures. In contrast, for tasks like News

[11] `https://github.com/princeton-nlp/Cognac/tree/main`

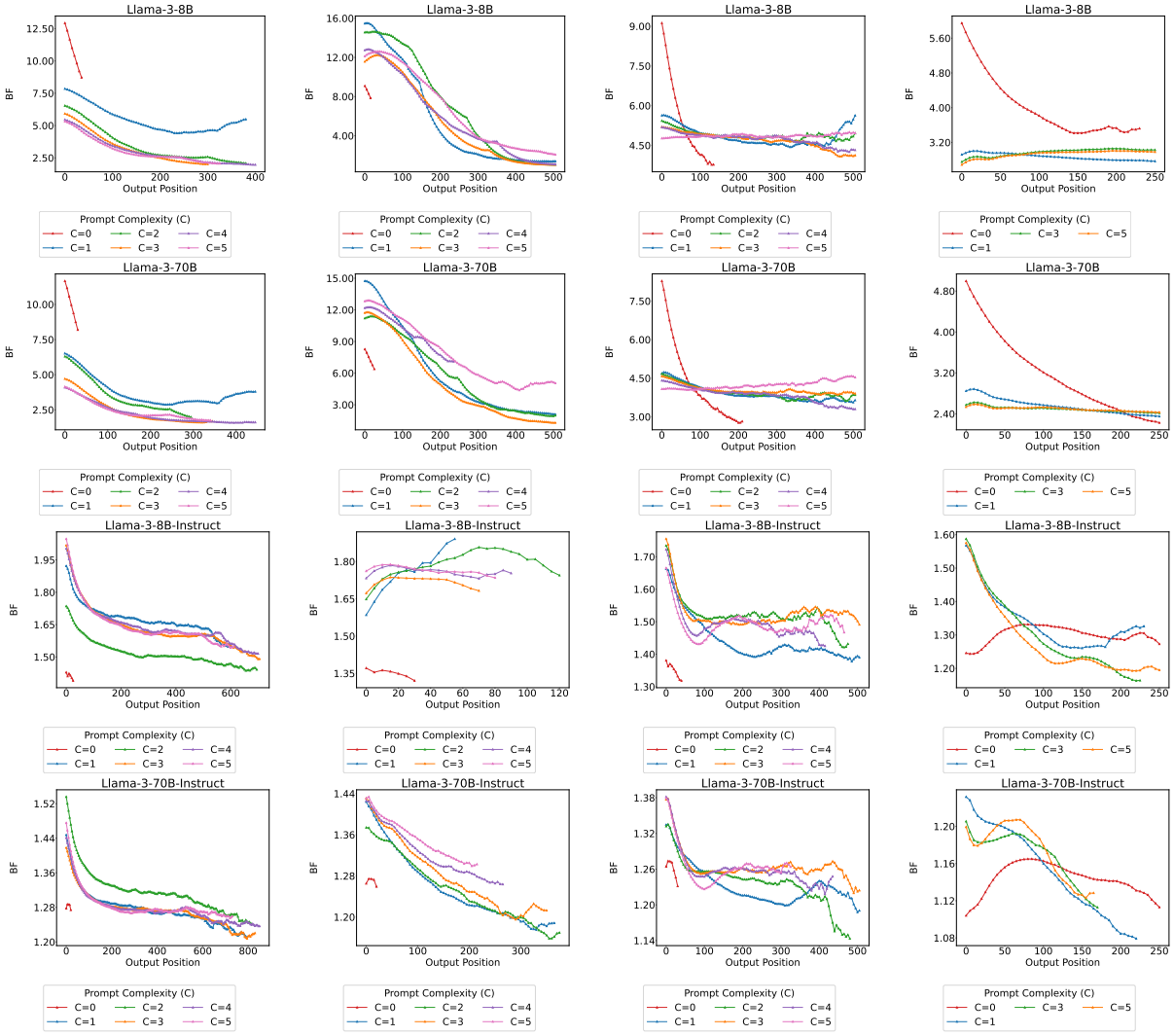

(a) Creative StoryGen (b) Random Strings (c) BBCNewsLatest (d) MMLU

Figure 11: **BF Output Dynamic for Llama-3-families.** For better visualization, we compute the exponential moving averaged values of perplexity with the smoothing factor set as 0.1.

Generation, higher C generally leads to lower BF, consistent with the expected narrowing of output diversity. Comprehensive task-wise BF results are provided in § F.

F Full Task-wise BF Evaluation on Different Prompt Complexity

The full task-wise BF evaluation results over different prompt complexity can be found in Figure 14. Here we can see that prompt complexity modulates BF in highly non-consistent ways across models and tasks, and there are no clear monotonic patterns, contradicting the intuition that with more context given, the model should have more confidence in what to generate.

G Generalization to Additional Tasks and Models

To confirm the generalizability of our findings (§ 4), we extend our experiments to new domains: summarization on XSUM (Narayan et al., 2018), multilingual tasks on Aya (Singh et al., 2024). We formulate prompt

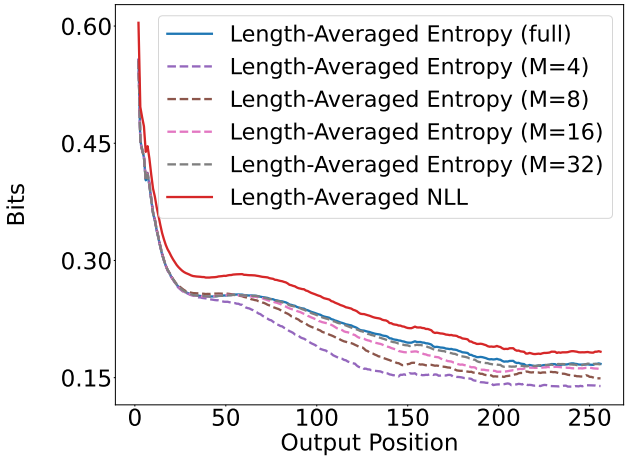

Figure 12: **Monte Carlo (MC) sampling systematically underestimates entropy.** The plot shows that the estimated entropy of sequences from Llama-3-8B-Instruct increases with the number of MC samples (M). A small sample size fails to cover the vast output space, leading to an underestimation of the true entropy. This bias is difficult to eliminate without incurring substantial computational costs.

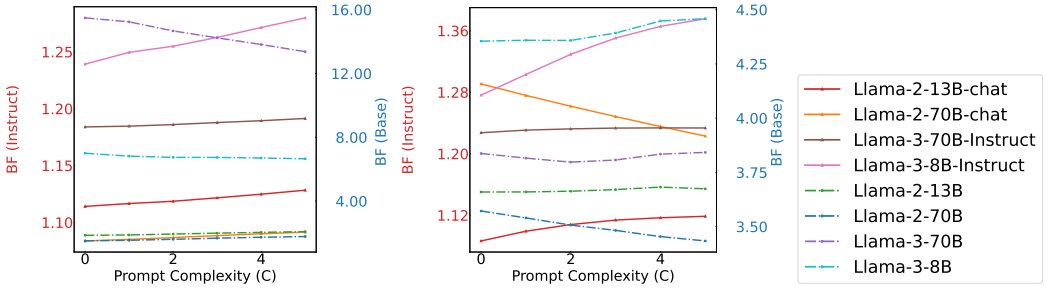

(a) Cognac (b) BBCNewsLatest

Figure 13: **Task-varied influence of prompt complexity C on BF.** On Cognac, we see BF increases with increased C, while on BBCNewsLatest, increasing C can lead to reduced BF.

complexity C as providing $C \times 25$ words in the prompt. We also verify our findings on a new model, Qwen3-4B (Qwen, 2025).[12] As presented in Figure 15, our core conclusions remain robust across these diverse conditions.

We also analyze OLMo-2 (OLMo et al., 2024) across different alignment stages (Base and DPO) on Creative StoryGen and MMLU, covering both 7B and 13B scales. As shown in Figure 16, OLMo-2 exhibits a similar trend where alignment tuning reduces BF, although the reduction is less pronounced compared to Llama models, suggesting that OLMo-2's post-training asserts less influence on the generation manifold. Additionally, we provide the BF dynamics for Qwen3-4B on MMLU in Figure 17.

H Proof of LLM Log-Likelihood Convergence

The following proof is a simplified version of the one in (Mudireddy et al., 2024), presented for completeness and to refine its original bounds. For the formal measure-theoretical treatment, we refer readers to the original paper. While a more direct proof using the weak law of large numbers is possible, we use Chebyshev's inequality to provide a more self-contained and accessible argument.

[12]For the Qwen3 family, we use the Qwen3-4B-Base and Qwen3-4B-Instruct-2507 pair. Other aligned variants can be activated into a reasoning mode, exhibiting behavior distinct from the models in our main study, and were thus excluded for a fair comparison.

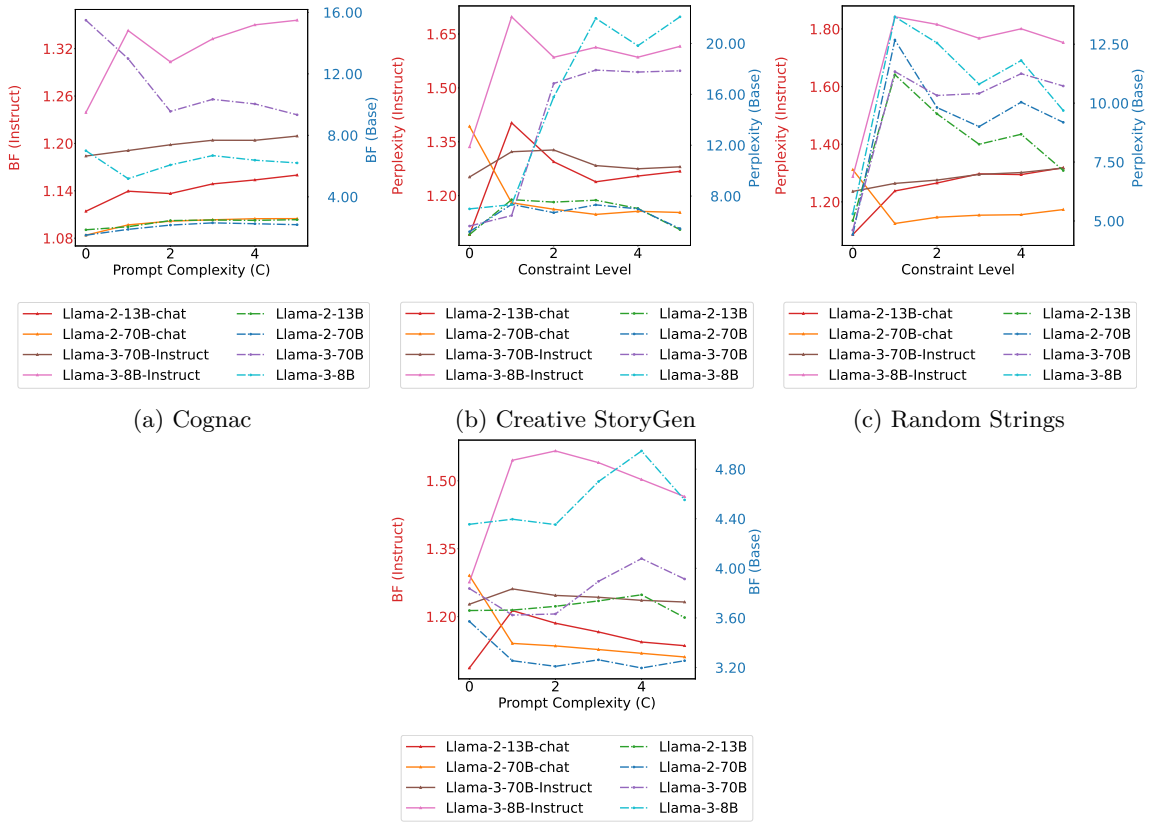

(a) Cognac (b) Creative StoryGen (c) Random Strings

(d) BBCNewsLatest

Figure 14: BF changes with prompt complexity (C) for Different Tasks. We can see prompt complexity affects BF in a task-varied way.

The key observation here is that under current computation architecture, the probability implemented by transformers are log-precision (Merrill & Sabharwal, 2023), and thus $|\log P(y_{1:N}|x;\theta)|$ is bounded (e.g., $|\log P(y_{1:N}|x;\theta)| \leq M$). For the truncated probability $\tilde{P}(y_{1:N}|x;\theta)$, we can essentially only consider the non-zero probability over the truncated vocabulary, and the same bound holds. Depending on the quantization scheme implemented, examples of M include $32, 64$, etc.

We define the length-averaged *realized entropy* for a specific sequence $y_{1:N}$ as:

$$h_{\text{realized}}(y_{1:N}) \stackrel{\text{def}}{=} \frac{1}{N}\sum_{t=1}^{N} H(\mathrm{Y}_t|[x, y_{<t}];\theta) \tag{10}$$

where $H(\mathrm{Y}_t|[x, y_{<t}];\theta) = -\sum_{y\in V} \tilde{P}(y|[x, y_{<t}];\theta)\log \tilde{P}(y|[x, y_{<t}];\theta)$.

We aim to bound the probability that the NLL deviates from this realized entropy. Let Δ_N be the total difference between the log-probability and the realized entropy sum:

$$\Delta_N = \left(-\log \tilde{P}(y_{1:N}|x;\theta)\right) - \sum_{t=1}^{N} H(\mathrm{Y}_t|[x, y_{<t}];\theta) = \sum_{t=1}^{N} Z_t \tag{11}$$

where we define the single-step deviation variable Z_t as:

$$Z_t \stackrel{\text{def}}{=} -\log \tilde{P}(y_t|[x, y_{<t}];\theta) - H(\mathrm{Y}_t|[x, y_{<t}];\theta) \tag{12}$$

Note that Δ_N is a random variable formed by the sum of Z_t. To use Chebyshev's inequality, we need to calculate the variance of this sum:

$$\mathrm{Var}(\Delta_N) = \mathrm{Var}\left(\sum_{t=1}^{N} Z_t\right) = \sum_{t=1}^{N}\mathrm{Var}(Z_t) + \sum_{i\neq j}\mathrm{Cov}(Z_i, Z_j) \tag{13}$$

We now show that the covariance terms $\mathrm{Cov}(Z_i, Z_j)$ are zero for all $i < j$. By definition, $\mathrm{Cov}(Z_i, Z_j) = \mathbb{E}[Z_i Z_j] - \mathbb{E}[Z_i]\mathbb{E}[Z_j]$.

First, observe that the expected value of the deviation Z_j at any step, conditioned on the prompt and generated history, is zero:

$$\begin{aligned}\mathbb{E}[Z_j|[x, y_{<j}];\theta] &= \mathbb{E}_{y_j}\left[-\log \tilde{P}(y_j|[x, y_{<j}];\theta)\right] - H(\mathrm{Y}_j|[x, y_{<j}];\theta) \\ &= H(\mathrm{Y}_j|[x, y_{<j}];\theta) - H(\mathrm{Y}_j|[x, y_{<j}];\theta) = 0\end{aligned} \tag{14}$$

This implies $\mathbb{E}[Z_j] = 0$ for all j. Thus, $\mathrm{Cov}(Z_i, Z_j) = \mathbb{E}[Z_i Z_j]$.

For $i < j$, the value of Z_i is fully determined by the history $[x, y_{<j}]$. We use the Law of Iterated Expectations, conditioning on the history up to step j:

$$\mathbb{E}[Z_i Z_j] = \mathbb{E}_{[x,y_{<j}]}\left[\mathbb{E}[Z_i Z_j|[x, y_{<j}];\theta]\right] \tag{15}$$

$$= \mathbb{E}_{[x,y_{<j}]}\left[Z_i \cdot \mathbb{E}[Z_j|[x, y_{<j}];\theta]\right] \quad \text{(since } Z_i \text{ is determined given } y_{<j}\text{)} \tag{16}$$

$$= \mathbb{E}_{[x,y_{<j}]}\left[Z_i \cdot 0\right] \quad \text{(by Eq. 14)} \tag{17}$$

$$= 0 \tag{18}$$

Since all cross-terms are zero, the variance of the sum is simply the sum of the variances:

$$\mathrm{Var}(\Delta_N) = \sum_{t=1}^{N}\mathrm{Var}(Z_t) \tag{19}$$

Given the observation that transformer probabilities are computed with bounded log-precision (Merrill & Sabharwal, 2023), we have $|\log P(y|[x, y_{<t}];\theta)| \leq M$ (For un-truncated P). Consequently, the random variable Z_t is bounded, and its variance is bounded by a constant, denoted $C = (2M)^2$.

$$\mathrm{Var}(\Delta_N) \leq N \cdot C \tag{20}$$

We can now apply Chebyshev's inequality to the length-averaged deviation:

$$P\left(\left|\frac{\Delta_N}{N}\right| \geq \epsilon\right) \leq \frac{\mathrm{Var}(\Delta_N/N)}{\epsilon^2} = \frac{\frac{1}{N^2}\mathrm{Var}(\Delta_N)}{\epsilon^2} \leq \frac{\frac{1}{N^2}(N \cdot C)}{\epsilon^2} = \frac{C}{N\epsilon^2} \tag{21}$$

Taking the limit as $N \to \infty$, the probability of deviation approaches 0. Thus, we have convergence in probability:

$$-\frac{1}{N}\log \tilde{P}(y_{1:N}|x;\theta) - h_{\text{realized}}(y_{1:N}) \xrightarrow{P} 0 \tag{22}$$

I Full Nudging Experiment Results

Due to space limits, we put the nudging experiment results for MMLU here. Though on MMLU, nudging does not reduce BF that quickly as over Just-Eval-Instruct, it does bring down BF of base models significantly, which verifies our hypothesis in § 6.

J BF and Information Density

Our BF measure can also be interpreted as capturing the information density that LLMs target to facilitate efficient communication (Genzel & Charniak, 2002; Jaeger & Levy, 2006; Levy, 2008; Mahowald et al., 2013; Meister et al., 2021; Verma et al., 2023). Prior work has leveraged both token-level log-probabilities and entropy rates ($\bar{H}$) as proxies for information density in human and machine communication. In Theorem 3.1, we formalize the connection between these views, showing that BF–defined as the exponentiated entropy rate–aligns naturally with this theoretical framework. Unlike prior studies focused primarily on linguistic theory or cognitive science, our work operationalizes this principle at scale across modern LLMs, linking information density to alignment training, decoding dynamics, and output variability in a unified analysis.

K Discussion: Diversity and BF Correlation

Following the branching factor (BF) analysis in § 2, a higher BF suggests greater lexical diversity in finite samples. To examine the relationship between BF and traditional diversity metrics, we compute Distinct-N (Li et al., 2016), incorporating necessary LLM-specific adaptations (Tevet & Berant, 2021; Guo et al., 2024; Kirk et al., 2024). We then conduct a correlation analysis between Distinct-N and BF.

Our results, presented in Figure 20, show **no consistent correlation** between BF and Distinct-N. Depending on the model and task, the relationship can be strongly positive, strongly negative, or entirely absent (e.g., Llama-3-70B-Instruct on Cognac at Figure 20b). This empirical inconsistency highlights a fundamental conceptual point: *BF measures a property of the underlying probability distribution, whereas diversity metrics measure a surface property of finite samples.*

BF, as the exponentiated entropy, characterizes the "width" of the model's entire output distribution. In contrast, metrics like Distinct-N describe a small set of sampled outputs and are known to be unreliable proxies for distributional properties, being sensitive to confounding factors like generation length (Liu et al., 2022).[13] This distinction is critical, as two models can produce samples of similar diversity while having fundamentally different underlying distributions (e.g., with infinite KL-divergence), a nuance that BF captures but sample-based metrics miss. Therefore, our work focuses on probability concentration, measured by BF, as a more fundamental and insightful tool for understanding a model's generative process.

Viewing alignment through the lens of BF reduction provides a unified framework that explains several disparate observations: it clarifies how alignment shrinks the generative horizon, why aligned models are less sensitive to decoding methods, and how techniques like Chain-of-Thought stabilize generation by shifting information to low-BF regions. This focus on distributional properties aligns with emerging research highlighting the importance of a model's entropy in understanding and improving advanced reasoning capabilities Cui et al. (2025); Wu et al. (2025b).

[13] While the EAD metric (Liu et al., 2022) mitigates this issue, it remains influenced by vocabulary size and is not model-agnostic.

L Confounder Investigation: Data Contamination

A potential confounder in our analysis is the influence of data contamination. If prompts closely resemble the training data (including pretraining and alignment tuning, i.e., "data contamination"), smaller BF values would be expected, and vice versa. To evaluate this, we use the Min-K% metric (Shi et al., 2024b), which quantifies the overlap between experimental prompts and training data. Following Shi et al. (2024b), we set $K = 20$ and compute the average log-likelihood for the minimum $K\%$ of tokens. Using these Min-K% values, we perform a linear regression with BF to assess their correlation. For each task-model pair, Signed R^2 values are reported to indicate the strength and sign (positive or negative) of the correlation.

The results of the Min-K% analysis are presented in Figure 21. Significant negative correlations between BF and Min-K% are observed for models such as Llama-3-8B-Instruct, Llama-3-70B-Instruct, and Llama-2-70B-Chat across several tasks. Conversely, Llama-3-8B and Llama-2-13B-Chat models exhibit positive correlations. For other models, correlations are notably weaker. Overall, there is no consistent correlation pattern between BF and Min-K% across datasets and models, suggesting that data contamination cannot fully explain our findings.

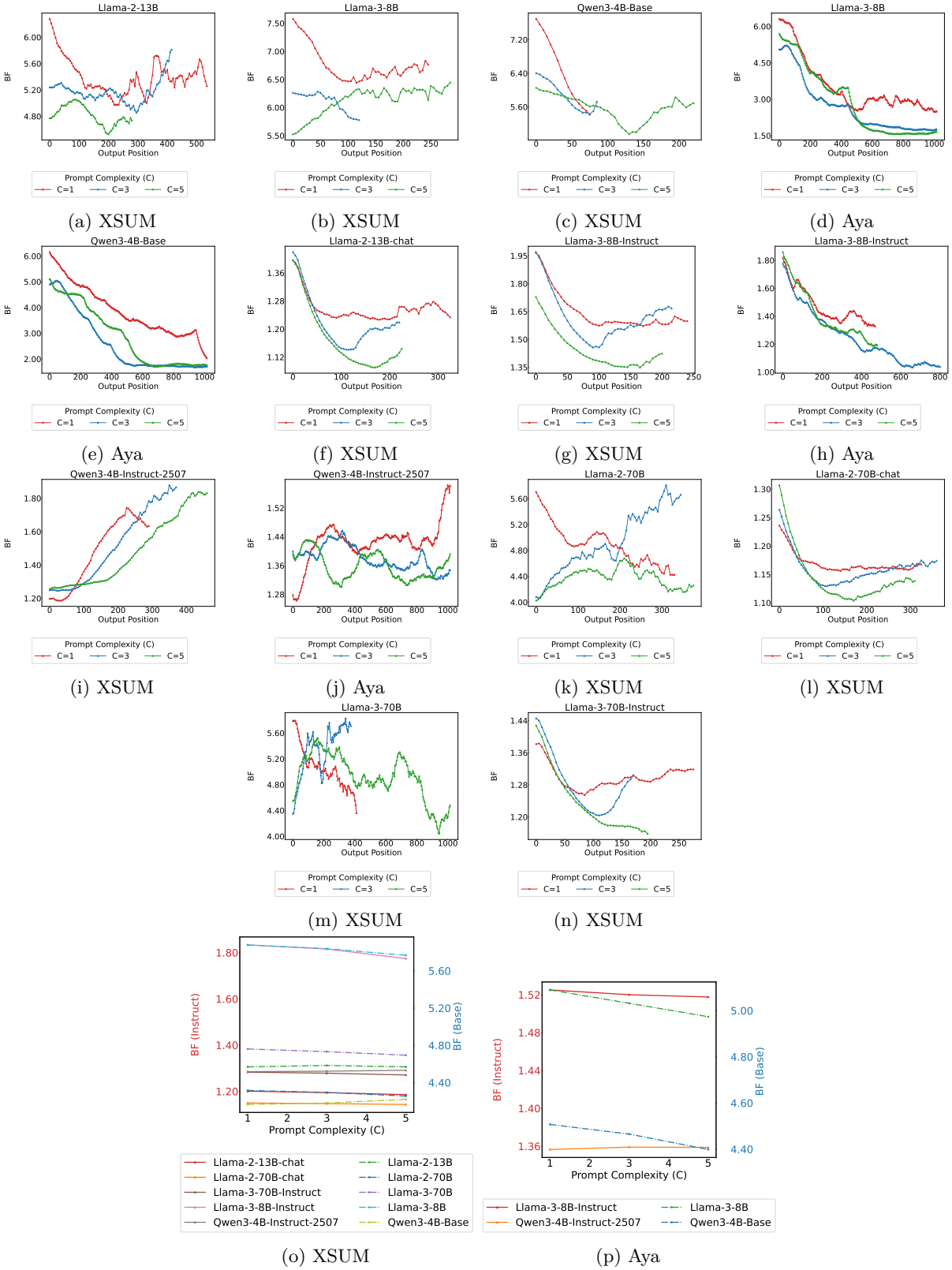

(a) XSUM (b) XSUM (c) XSUM (d) Aya

(e) Aya (f) XSUM (g) XSUM (h) Aya

(i) XSUM (j) Aya (k) XSUM (l) XSUM

(m) XSUM (n) XSUM

(o) XSUM (p) Aya

Figure 15: **Additional Verification on Summarization, Multilingual and Qwen Model family.** For better visualization, we compute the exponential moving averaged values of perplexity with the smoothing factor set as 0.1.

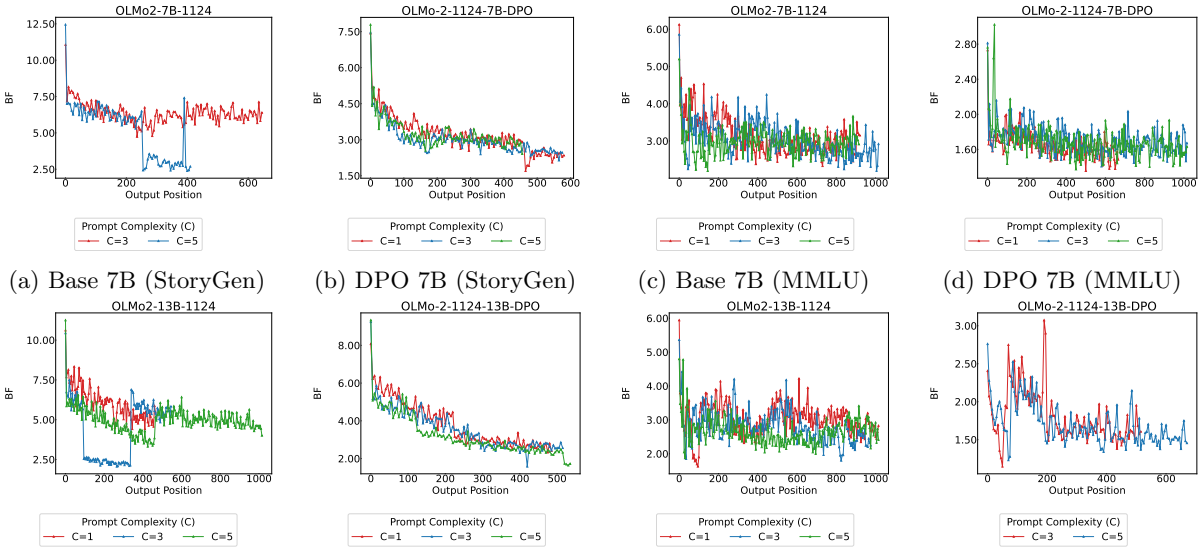

(a) Base 7B (StoryGen) (b) DPO 7B (StoryGen) (c) Base 7B (MMLU) (d) DPO 7B (MMLU)

(e) Base 13B (StoryGen) (f) DPO 13B (StoryGen) (g) Base 13B (MMLU) (h) DPO 13B (MMLU)

Figure 16: **BF Output Dynamic for OLMo-2 (7B & 13B) across alignment stages.** We compare Base and DPO models on Creative StoryGen and MMLU. Note that we treat DPO as the aligned model for OLMo-2, following the convention in (OLMo et al., 2024).

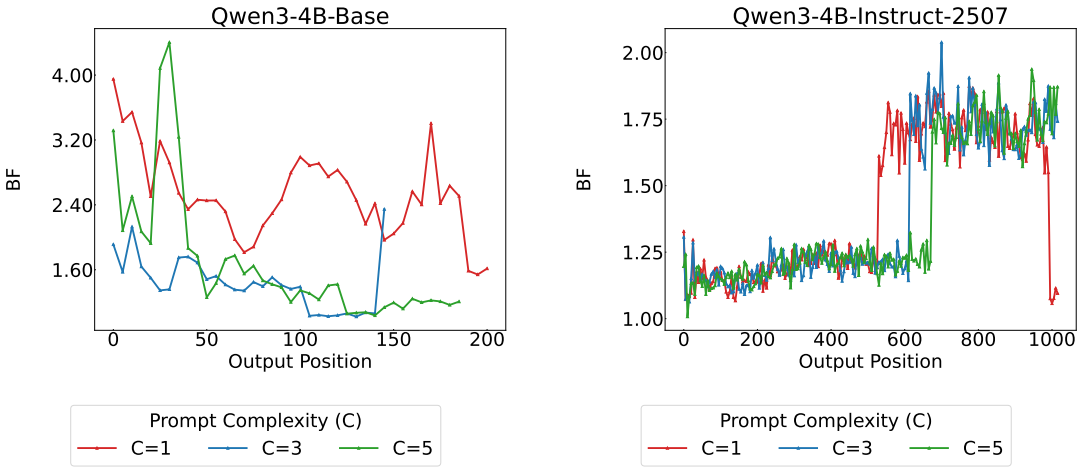

(a) Qwen3-4B-Base (MMLU) (b) Qwen3-4B-Instruct (MMLU)

Figure 17: **BF Output Dynamic for Qwen3-4B on MMLU.**

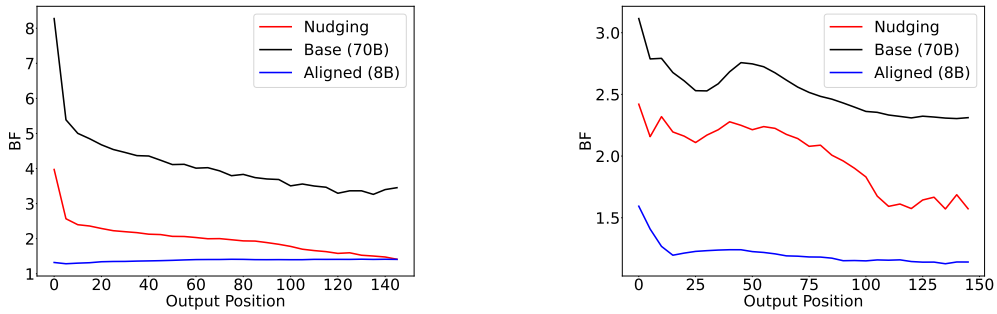

(a) Just-Eval-Instruct (b) MMLU

Figure 18: Output Perplexity Dynamics in Nudging Experiments.

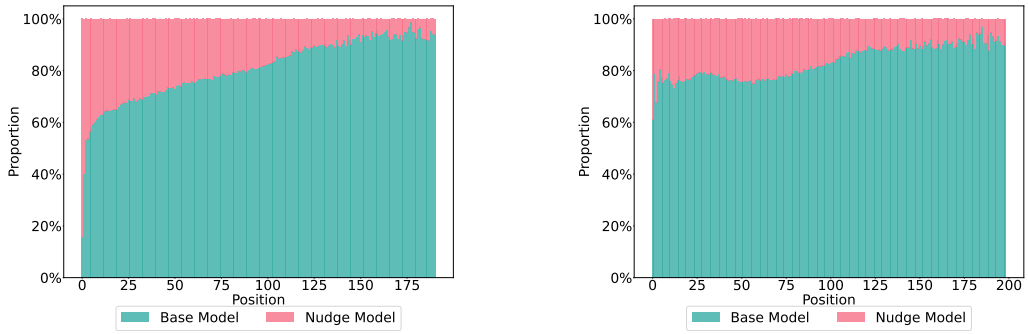

(a) Just-Eval-Instruct (b) MMLU

Figure 19: Nudging Ratio Histogram.

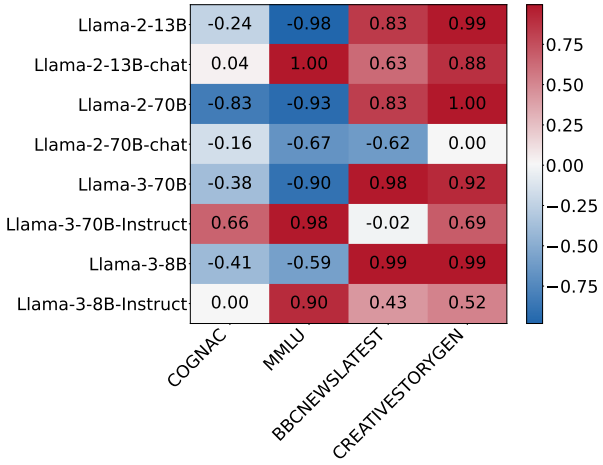

(a) Signed R^2(Distinct-1, BF), MaxLength=5

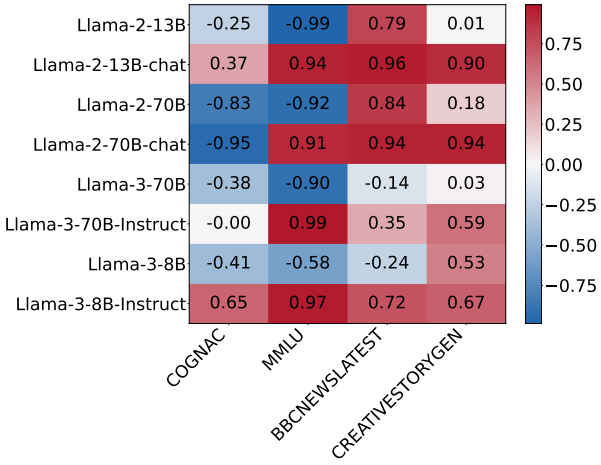

(b) Signed R^2(Distinct-1, BF), MaxLength=50

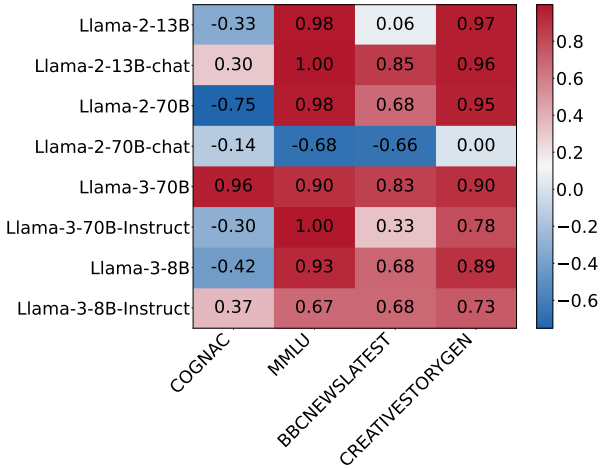

(c) Signed R^2(Distinct-2, BF), MaxLength=5

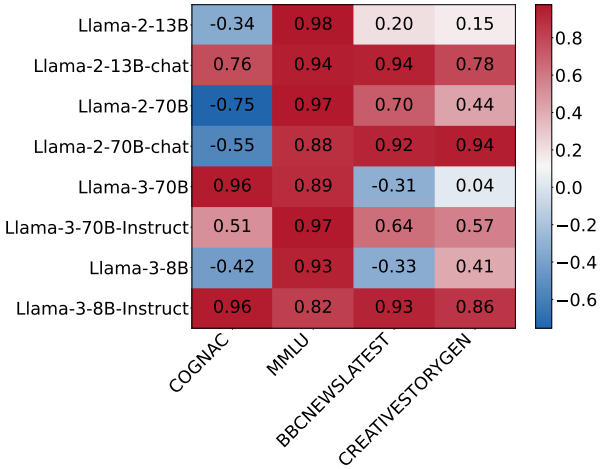

(d) Signed R^2(Distinct-2, BF), MaxLength=50

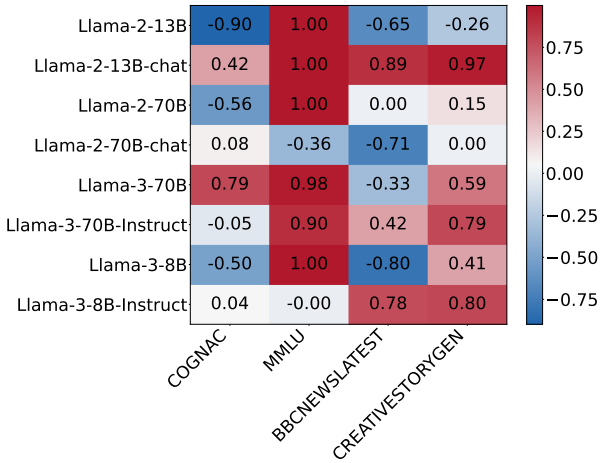

(e) Signed R^2(Distinct-4, BF), MaxLength=5

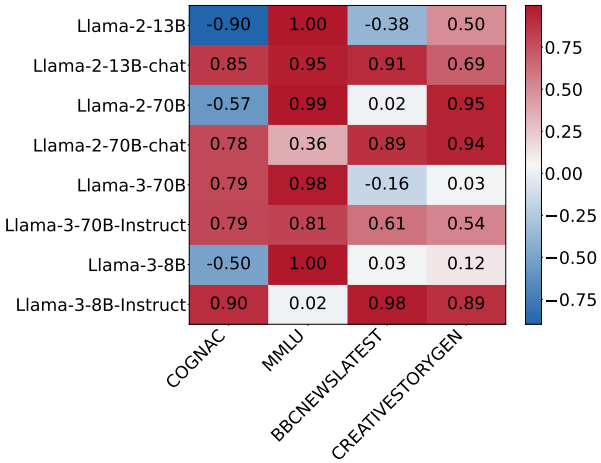

(f) Signed R^2(Distinct-4, BF), MaxLength=50

Figure 20: Correlational Analysis of BF and Distinct-N. We can find there is no consistent correlation between Distinct-N and BF.

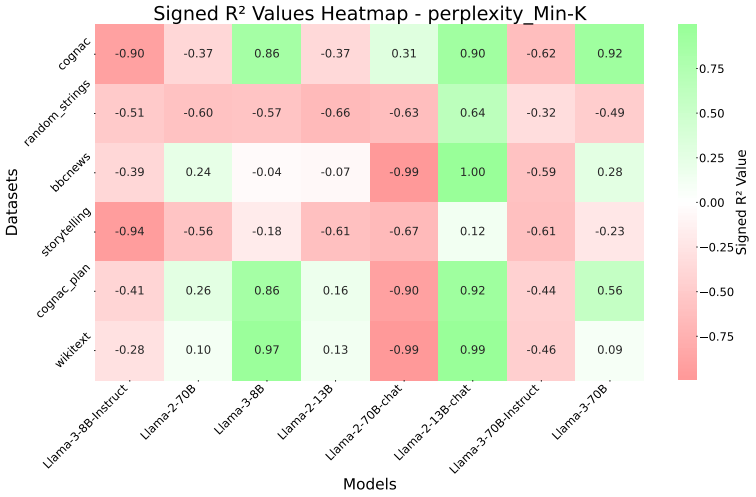

Figure 21: Signed R^2 values heatmap investigating correlation between BF and Min-K %.